R009-01
Zoom meeting D ：11/1　AM1　(9:00-10:30)
09:00-09:15

ベピコロンボ水星探査計画の最新状況：惑星間空間航行およびフライバイの初期結果と今後の観測計画

#村上　豪 BepiColombo MMO SWG　村上 豪
JAXA/ISAS,[2)]ESA

Updated status of BepiColombo: results and observation plan of interplanetary cruise and flybys

#Go Murakami, Johannes Benkhoff[2)], Go Murakami BepiColombo MMO SWG
JAXA/ISAS,[2)]ESA

The ESA-JAXA joint mission BepiColombo is now on the track to Mercury. After the successful launch of the two spacecraft for BepiColombo, Mio (Mercury Magnetospheric Orbiter: MMO) and Mercury Planetary Orbiter (MPO), commissioning operations of the spacecraft and their science payloads were completed. BepiColombo will arrive at Mercury in the end of 2025, and it has 7-years cruise with the heliocentric distance range of 0.3-1.2 AU. The long cruise phase also includes 9 planetary flybys: once at the Earth, twice at Venus, and 6 times at Mercury. Even during the interplanetary cruise phase, the BepiColombo mission can contribute to the heliospheric physics and planetary space weather in the inner solar system. In addition, NASA's Parker Solar Probe was launched in 2018 and it is orbiting around Sun (~0.05 AU at perihelion). ESA's Solar Orbiter was launched in February 2020 and will have a highly elliptic orbit between 1.2 AU at aphelion and 0.28AU at perihelion. These multi spacecraft observations provide us great opportunities to investigate the inner heliosphere. The first Earth flyby was successfully completed on 10 April 2020. The spacecraft crossed the Earth's magnetosphere and thus it was a great opportunity to calibrate and test the instrument performances onboard Mio and MPO. The next Venus flyby will happen on 15 October 2020 and the Mio spacecraft will observe the plasma environments around Venus which is highly interacted with the solar wind. Here we present the updated status of BepiColombo mission, initial results of the science observations during the interplanetary cruise and planetary flybys, and the upcoming observation plans.

R009-02
Zoom meeting D ：11/1　AM1　(9:00-10:30)
09:15-09:30

水星の表面組成異常と外気圏組成分布の関係性

#鈴木　雄大[1)],吉岡　和夫[1)],村上　豪[2)],吉川　一朗[1)]
[1)]東京大学,[2)]ISAS/JAXA

Relation between the surface composition anomaly and the distribution of the exosphere of Mercury

#Yudai Suzuki[1)], Kazuo Yoshioka[1)], Go Murakami[2)], Ichiro Yoshikawa[1)]
[1)]The Univ. of Tokyo,[2)]ISAS/JAXA

In celestial bodies with thin atmosphere, such as Mercury and Moon, atoms in the exosphere are mainly supplied by the desorption from the surface. Since these atmosphere is regarded as collision-less, the surface composition distribution could be directly reflected in the distribution of the exosphere. In the previous study, Merkel et al. (2018), the amount of Mg exosphere on Mercury is turned out to be enhanced above Mg-rich terrain, using the observational data by MASCS and XRS, both of which were onboard MESSENGER spacecraft. If this exosphere-surface composition correlation exists universally in other atoms and other celestial bodies, we would be able to estimate the surface composition distribution from remote observations of the exosphere.
Na, Ca, and Mg in the Mercury's exosphere were observed by MASCS onboard MESSENGER. The surface distribution of Na has been estimated by a model of thermal desorption using observational data in limited regions. Highly volatile Na is thought to repeat the ejection from the surface and the re-impact on the surface, and accumulates on low temperature regions. Therefore, it has been expected that the surface composition distribution does not correlate to topography and the exosphere distribution reflects the temperature distribution. The surface Ca distribution, on the other hand, does not drastically vary due to the low volatility, as well as Mg, we have expected that the enhancement of the exosphere would be seen above certain topographies.
Our study aims to understanding the conditions of atomic species and celestial bodies that show the exosphere-surface correlation. We applied the analysis method by Merkel et al. (2018) to Ca and Na, and analyzed MESSENGER data to verify the correlation of the surface density distribution and the production rate of the exosphere. As a result, we unexpectedly found that there is no correlation between the distribution of the exosphere and the surface density for Ca. One of the causes of the difference in the results of Mg and Ca is thought to be the difference in the magnitude of solar radiation acceleration. Because the resonance scattering efficiency (g-factor) of Ca is higher than that of Mg, it is likely to be accelerated in the anti-sunward by solar radiation. Therefore, the information on the surface density distribution, which is retained in the near-surface exosphere, may be easily diffused. We also constructed 3-D model of Ca and Mg exosphere of Mercury to evaluate the contribution of solar radiation to the exosphere's structure. On the other hand, it was found that there was a difference in the Na production rate even in the regions with the same temperature environment. This result implies that surface density anomaly due to the large meteorite impact and so on should be kept, even if the surface Na density distribution varies due to the temperature gradient.
In future study, we will perform the same analysis for Moon and verify the exosphere-surface correlation on other celestial bodies with thin atmosphere.

水星や月などの希薄大気保持天体では、主に天体表面からの脱離によって大気中に原子が供給される。これらの天体の大気は非常に希薄であり、無衝突と見做せるため、表面密度分布が大気構成原子の分布に直接反映されている可能性がある。Merkel et al., 2018 では、MESSENGER 探査機搭載の分光観測装置 MASCS による大気分布の観測データおよび X 線分光器 XRS による表面組成分布の観測データの解析から、水星において大気中の Mg 量が表面の Mg に富んだ平地の上空で増加していることが分かった。この大気・表面組成相関が他原子や他天体においても普遍的に存在するならば、希薄大気保持天体の大気の遠隔観測から表面組成分布を推定可能になると期待できる。
MESSENGER/MASCS により水星外気圏中の Na, Ca, Mg の分布が観測された。Na の表面分布は限られた領域の観測データを利用した熱脱離のモデルにより推定されてきたが、揮発性の高い Na は、熱脱離による表面からの低エネルギー粒子の放出と表面への再衝突を繰り返して低温領域に濃集すると考えられている。従って、地形情報は表面組成分布には反映されず、大気分布は水星表面の温度分布を反映していると考えられてきた。一方で、Ca は Mg 同様揮発性が低く表面分布が変動しにくいため、特定の地形の上空で大気量の増大が見られると期待されていた。
本研究では、大気・表面組成相関が見られる原子種および天体の条件の理解を目指し、Merkel et al., 2018 の手法を水星の Ca, Na に対しても適用し、表面組成分布と大気生成量の間の相関関係を調べた。その結果、Ca については予想に反して大気・表面組成分布の間に相関が見られないことが分かった。Mg と Ca の大気・表面組成相関の有無の違いの原因の 1 つとして、太陽放射圧による加速度の大きさの差異が挙げられる。Ca は Mg に比べて共鳴散乱効率（g-factor）が大きいため、太陽放射により反太陽方向に加速されやすく、表面付近の大気では保持されていた表面組成分布の情報が拡散しやすい可能性が考えられる。水星大気中の Ca, Mg の 3 次元力学モデルを用いて、これらの原子の大気中での挙動に対する太陽放射の寄与も評価した。一方で、Na については同じ温度環境にある領域の間で

も大気放出量に差があることが分かった。この結果からは、温度勾配による Na の表面組成分布の変化が生じてもなお、巨大隕石衝突等に由来する地形に対応した表面組成異常が見られる可能性が窺える。
今後の研究では月に対しても同様の解析を行い、他天体における大気・表面組成分布の相関の有無を検証する。

R009-03
Zoom meeting D ：11/1　AM1　(9:00-10:30)
09:30-09:45

BepiColombo Mio 搭載イオンエネルギー分析器 MPPE-MIA の軌道上性能評価

#齋藤　義文[1)],原田　裕己[2)],横田　勝一郎[3)],三宅　亙[4)]
[1)]宇宙研,[2)]京大・理・地球惑星,[3)]阪大,[4)]東海大・工

Evaluation of the in-flight performance of MPPE-MIA on BepiClombo/Mio

#Yoshifumi Saito[1)], Yuki Harada[2)], Shoichiro Yokota[3)], Wataru Miyake[4)]
[1)]ISAS,[2)]Dept. of Geophys., Kyoto Univ.,[3)]Osaka Univ.,[4)]Tokai Univ.

BepiColombo Mio was successfully launched by Ariane 5 from Kourou, French Guiana on 20 October 2018. The Mercury Plasma/Particle Experiment (MPPE) is a comprehensive instrument package on Mio spacecraft for plasma, high-energy particle and energetic neutral atom measurements. It consists of 7 sensors: two Mercury Electron Analyzers (MEA1 and MEA2), Mercury Ion Analyzer (MIA), Mass Spectrum Analyzer (MSA), High Energy Particle instrument for electron (HEP-ele), High Energy Particle instrument for ion (HEP-ion), and Energetic Neutrals Analyzer (ENA). MIA that measures 3D phase space density of low energy ions between 15eV/q and 29keV/q was developed for understanding (1) structure of the Mercury magnetosphere, (2) plasma dynamics of the Mercury magnetosphere, (3) Mercury - solar wind interaction, (4) atmospheric abundances, structure, and generation/loss process, and (5) solar wind between 0.3 and 0.47 AU. In order to achieve these science objectives, MIA was designed to measure the three-dimensional distribution function of both solar wind ions around Mercury, and Mercury magnetospheric ions.
The low voltage part of MIA was turned on for the first time on 25 November 2018 about one month after the launch. No problems were identified during the low voltage function tests including calibration pulse injected into all the channels of the pre-amplifier. The high voltage tests were performed on 3 and 4 July 2019 about 8 months after the launch when Mio was in the solar wind. High voltage up to +2500V, -3610V, -2471V were successfully tested for SVG (stepping high voltage power supply connected to “top-cap"), SVS (stepping high voltage power supply connected to the inner sphere) and MHV (high voltage power supply connected to the MCP detector), respectively. Dark counts of the MCP were observed indicating that the detector part of MIA was functioning normally. Since Mio is surrounded by MOSIF (MMO Sunshield and Interface Structure) during the cruise phase, most part of the MIA's field of view is blocked by MOSIF. No solar wind ions are observed since solar wind ion thermal velocity is much lower than the solar wind bulk velocity and MOSIF blocks the solar wind ions from entering into MIA.
Between 9 and 11 April 2020, BepiColombo made the first and last Earth fly-by. MIA made observation of low energy ions for about 19 hours on 10 and 11 April. Although most part of the MIA's field of view was blocked by MOSIF, MIA succeeded in measuring hot plasmas in the Earth's magnetosphere that entered MIA from topside of the Mio spacecraft. The obtained data were used for evaluating the in-flight performance of MIA. Most of the obtained data were as expected except for the onboard calculated velocity moments that were calculated unexpectedly by using a dummy table due to the lack of a few necessary commands.
MIA will be turned on again during Venus fly-by in October 2020. It is another good opportunity to keep remembering the instrument operation as well as a good opportunity to evaluate the performance of the instrument. The operation will be much improved by reflecting the results of Earth fly-by operation. During another Venus fly-by scheduled in August 2021, and during the Mercury fly-bys scheduled in October 2021, June 2022, June 2023, September 2024, December 2024 and January 2025, MIA will be turned on. The observation with full performance of MIA will start after Mio's arrival at Mercury in 2025.

BepiColombo Mio は 2018 年 10 月 20 日にフランス領ギアナのクールーからアリアン 5 によって打ち上げられた。MPPE（Mercury Plasma/Particle Experiment）は Mio 衛星に搭載された、プラズマ・高エネルギー粒子・高速中性粒子の計測を行う観測装置で、7 台の観測装置で構成されている。 2 台の電子計測センサー：Mercury Electron Analyzers (MEA1 and MEA2)，イオン計測センサー：Mercury Ion Analyzer (MIA)，イオン質量分析器：Mass Spectrum Analyzer (MSA)，高エネルギー粒子計測装置：High Energy Particle instrument for electron (HEP-ele)及び High Energy Particle instrument for ion (HEP-ion)と、高速中性粒子計測装置　Energetic Neutrals Analyzer (ENA)である。このうち、MIA は、15eV/q から 29keV/q の低エネルギーイオンの三次元分布関数の計測を行うことで（1）水星磁気圏の構造（2）水星磁気圏におけるプラズマのダイナミクス（3）水星と太陽風の相互作用（4）水星希薄大気の組成、構造、生成・消滅過程（5）0.3AU　から 0.47 AU における太陽風の理解を目指す。これらの科学目的を達成するために、MIA は水星周辺の太陽風イオンと、水星磁気圏イオン両方の三次元分布関数を計測できるように設計した。
　MIA の低電圧部分は、打ち上げ約 1 ヶ月後の 2018 年 11 月 25 日に初めて立ち上げ、プリアンプの全チャンネルに較正パルスを入力するなどし、特に問題無く試験を完了することができた。打ち上げ約 8 ヶ月後の 2019 年 7 月 3 日と 4 日には太陽風中で高圧の試験を実施した。3 台の高圧 SVG（感度制御用高圧）、SVS（エネルギー分析用高圧）、MHV（検出器用高圧）にそれぞれ最大で+2500V, -3610V, -2471V を印加し、問題の無いことを確認した。検出器の MCP（Micro Channel Plate）に高圧を印加すると、正常にダークカウントが検出され、MIA の検出器が正常に動作していることが確認できた。Mio 衛星はクルージングフェーズの間、サーマルシールド MOSIF (MMO

Sunshield and Interface Structure)に囲まれているため、MIA の殆どの視野は MOSIF によって遮られてしまう。太陽風の熱速度は太陽風プラズマ全体の速度よりも低いことから、太陽風イオンは MOSIF に遮られて観測することができない。

2020 年 4 月 9 日から 11 日にかけて BepiColombo は最初で最後の地球フライバイを行ったが、その際に MIA は 4 月 10 日と 11 日の 2 日間、約 19 時間に渡って低エネルギーイオンの観測を行った。MIA の視野は殆どが MOSIF に遮られているものの、MIA は Mio 衛星の上方から飛来する地球磁気圏のイオンを計測することに成功した。得られたデータを用いて MIA の軌道上観測性能の評価を行ったが、殆どのデータは期待通りのものであった。唯一、速度モーメントがダミーの情報テーブルを用いて計算されてしまったことが想定外であったが、これは必要なコマンドをいくつか実行し忘れていたことに起因することが明らかとなっている。

MIA は 2020 年 10 月に予定されている金星フライバイの際にも再び観測を行う予定あるが、フライバイの機会は観測装置の性能評価を行うための良い機会であることに加えて、観測装置の運用を忘れないためにも重要な機会である。今回の地球フライバイの際に学んだことを反映して、金星フライバイの際の運用はより円滑に行えることが期待できる。その後 2021 年 8 月に予定されている 2 回目の金星フライバイと 2022 年 6 月、2023 年 6 月、2024 年 9 月、2024 年 12 月に予定されている水星フライバイの際にも MIA は観測を行う予定であるが本格的な観測を開始するのは、2025 年 12 月に Mio 衛星が水星に到着してからの予定である。

R009-04
Zoom meeting D ：11/1　AM1　(9:00-10:30)
09:45-10:00

「かぐや」によって観測された月起源二次イオンと月表面組成の関係

#江川　喜啓[1)],齋藤　義文[2)],西野　真木[3)],横田　勝一郎[4)],高橋　太[5)],清水　久芳[6)]
[1)]東大地惑,[2)]宇宙研,[3)]JAXA,[4)]阪大,[5)]九大・理・地惑,[6)]東大・地震研

Relation between lunar surface composition and the Moon originating secondary ions observed by Kaguya

#Yoshihiro Egawa[1)], Yoshifumi Saito[2)], Masaki N Nishino[3)], Shoichiro Yokota[4)], Futoshi Takahashi[5)], Hisayoshi Shimizu[6)]
[1)]eps,u-tokyo,[2)]ISAS,[3)]JAXA,[4)]Osaka Univ.,[5)]Kyushu Univ.,[6)]ERI, University of Tokyo

Since the Moon does not have thick atmosphere and global magnetic field, lunar surface is exposed to the solar wind when it is outside the Earth's magnetosphere. Secondary ions are emitted by the solar wind ions and sunlight colliding with the lunar surface. The generated secondary ions have energy of only several electron volts, but the energy increases up to several hundred electron volts while being accelerated by the solar wind convection electric field and the accelerated ions can be detected by satellites on lunar orbit. It is expected that the composition of the secondary ions which was produced by the solar wind sputtering corresponds to the lithofacies and elemental composition of the place where the secondary ions are generated. However, the interaction between solar wind ions and solids on the surface of the Moon and the distribution of secondary ions around the Moon have not been understood well.
MAP-PACE-IMA on Kaguya performed energy and mass observation of the Moon origin ions. Using IMA data, we investigated the dependence of the secondary ion measurements on the production sites of the major elements (Mg, Si, Fe) that compose the rocks on the lunar surface. The secondary ions are thought to be generated by the solar wind ion collision on the Moon. In order to select only the ions generated near lunar surface and determine the location where the secondary ion are generated, we used the data of MAP-PACE-IEA: ion energy analyzer and MAP-LMAG: lunar magnetometer on Kaguya. We calculated the solar wind convection electric field and the generation point of the secondary ions was determined by tracing back the ion location from the ion observation point along the solar wind electric field. In order to understand the relationship between the composition of the lunar surface and the generated secondary ions, we have compared the ratio of magnesium ion to silicon ion (Mg+/Si+) and iron ion to silicon ion (Fe+/Si+) in order to eliminate the influence of solar wind ion flux intensity as much as possible.
Since the lunar mare region contains more magnesium and iron than the highlands, it is expected that more magnesium ions and iron ions are produced as the secondary ions by the solar wind sputtering. As a result of comparison between South Pole Aitken Terrane (SPAT) and the highlands on the lunar far side, we have found that Fe+/Si+ is higher in SPAT than in the highlands. We will report the method and the result of data processing including the correction of instrumental noise, and the results obtained regarding the dependence of Mg+/Si+ and Fe+/Si+ on the lunar surface location.

月は十分な大気と全球的な固有磁場を持たないため、地球磁気圏外に存在するとき、月面は太陽風にさらされている。このとき太陽風イオンや太陽光が月面に衝突することで二次イオンが放出される。生成された二次イオンは数 eV 程度のエネルギーしか持たないが、太陽風中の電場により数 100eV 程度まで加速されながら上昇し、月周回軌道上の衛星で観測することができる。ここで、太陽風イオンのスパッタリングにより生成される二次イオンの組成は生成された場所の岩相や元素組成に対応していることが期待される。しかしながら、太陽風イオンと月表面の固体物質の相互作用とその結果放出される二次イオンの月周辺における分布について未だよく理解されていない。
月探査衛星「かぐや」に搭載されたイオン観測装置 MAP-PACE-IMA は月起源のイオンのエネルギーと質量の分析を行った。本研究では IMA のデータを用いて、太陽風イオンの月面衝突で生成されると考えられる二次イオンのうち、月表面の岩石を構成する主要な元素(Mg、Si、Fe)について、二次イオンの計測量の生成場所に対する依存性を調べた。二次イオンの生成場所を決定し月表面付近で生成されたイオンのみを選択するにあたっては、「かぐや」に搭載された太陽風イオンのエネルギースペクトルを計測する観測装置 MAP-PACE-IEA のデータと磁力計 MAP-LMAG のデータを用いて太陽風電場を算出し、二次イオンの観測地点から太陽風電場に沿ってイオンの飛来方向を逆トレースした。また、月表面物質の組成や表層環境と生成される二次イオンの関係を理解するために、太陽風強度の影響をできるだけ取り除くべく、ケイ素イオンに対するマグネシウムイオン(Mg+/Si+)や鉄イオン(Fe+/Si+)の相対量の比較を行った。
月の海の領域では高地の領域に比べ、マグネシウムや鉄が多く含まれているので、生成されるマグネシウムイオンや鉄イオンも多いことが期待される。これまでに、月の裏側領域において南極エイトケン盆地と高地の領域を比較した結果、Fe+/Si+が南極エイトケン盆地で高地に比べ高いという結果が得られつつある。本発表では、質量分析器のデータに含まれるノイズデータの評価及びそれらの補正によるデータ処理の手法・結果と、Mg+/Si+と Fe+/Si+の月表面の生成領域に対する依存に関して得られた結果について報告する。

R009-05
Zoom meeting D ：11/1 AM1 (9:00-10:30)
10:00-10:15

Discrete rising tone elements of whistler-mode waves observed by ARTEMIS in the vicinity of the Moon

#Wataru Sawaguchi[1)], Yuki Harada[2)], Satoshi Kurita[3)]
[1)]Dept. of Geophys., Kyoto Univ.,[2)]Dept. of Geophys., Kyoto Univ.,[3)]RISH, Kyoto Univ.

Whistler-mode chorus emissions are narrow band electromagnetic emissions typically with rising tone elements in a frequency range of 0.2 - 0.8 f_{ce}, where f_{ce} is the electron cyclotron frequency. They are mostly observed in the Earth's inner magnetosphere, and also known to occur in the magnetospheres of Jupiter, Saturn and Mars. However, they have not yet been reported around airless bodies.
Although the Moon does not have a global, intrinsic magnetic field and a dense atmosphere, interaction of plasmas in the solar wind and in the Earth's magnetotail with the lunar surface and crustal magnetic fields causes various plasma phenomena. Whistler-mode waves can be excited in the vicinity of the Moon as a result of cyclotron resonance of waves traveling toward the Moon with upward electrons magnetically mirrored from the lunar surface. A free energy source for the wave excitation is provided by effective temperature anisotropy in electron velocity distribution functions resulting from the surface absorption of parallel electrons and magnetic reflection of perpendicular electrons. As these whistler-mode waves around the Moon can have as large amplitudes as those in the Earth's magnetosphere, they might possibly grow like chorus emissions.
We report the existence of discrete rising-tone elements of whistler-mode waves observed by ARTEMIS in the vicinity of the Moon along with results of two ways of analysis: two-point observations and data-theory comparison. To check if they are related to the Moon, we compare wave spectra, electron pitch angle distributions and magnetic connection to the lunar surface observed by one probe (foreground) with those observed by the other probe (background). These two-point observations demonstrate that the observed whistler mode waves are indeed moon-related as suggested by previous studies. Furthermore, we compare the frequency sweep rates of the observed rising-tone elements with those predicted by the nonlinear theory of chorus emissions by Omura et al. (2008). Based on the theory, relationship of sweep rates and wave amplitudes are estimated from the observed electron distributions and magnetic field strength. The predictions show a good agreement with the observations. These results imply that moon-related whistler-mode waves can grow nonlinearly into chorus-like emissions.

R009-06
Zoom meeting D ：11/1 AM2 (10:45-12:30)
10:45-11:00

The water production rate and D/H ratio around comet measured by the Comet Interceptor mission

#Kazuo Yoshioka[1)], Masaki Kuwabara[2)], Go Murakami[2)], Shingo Kameda[4)], Yudai Suzuki[3)], Makoto Taguchi[4)], Takuya Kawahara[5)], Ichiro Yoshikawa[1)]
[1)]The Univ. of Tokyo,[2)]ISAS/JAXA,[3)]Earth & Planetary Science, Univ. Tokyo.,[4)]Rikkyo Univ.,[5)]Faculty of Engineering, Shinshu University

Water (H2O) is a key material of the small bodies in the solar system that holds the information about the evolution of the solar system and the possibility of life. In many cases, the water inside a celestial body (comets or asteroids) is ejected from the surface or into space by sunlight or tidal heating, and then dissociated into hydrogen atoms and hydrogen oxide by UV light. Therefore, it is important to understand the spatial distribution and isotopic composition of these secondary products to understand the origin of the solar system. Although the size of a typical comet nucleus is only about 10 km, the hydrogen gas surrounding the nucleus (coma) is known to extend over 10 million km. We are developing a method to derive the density distribution and isotope ratio (D/H ratio) of hydrogen gas in the comet coma through remote observation. Specifically, the density distribution can be derived using the Lyman- α emission line from hydrogen and deuterium. In addition, an optical filter which is called as an absorption cell is placed on the light path to distinguish the hydrogen and deuterium Lyman- α. In this presentation, we will introduce the instrumentation of the Hydrogen Imager (HI) being designed for the ESA's “Comet Interceptor" mission. The feasibility of the remote observation by HI will also be discussed.

R009-07
Zoom meeting D ：11/1　AM2　(10:45-12:30)
11:00-11:15

宇宙空間へつながる木星大気の屋根を探る -- 「COMICS 最終観測」を含むすばる望遠鏡観測成果

#笠羽　康正[1)],北　元[2)],垰　千尋[3)],坂野井　健[1)],佐藤　隆雄[4)],藤吉　拓哉[5)],Sinclair　J.A.[5)],Orton　G.S.[5)]
[1)]東北大・理,[2)]東北工大,[3)]情報通信研究機構,[4)]北海道情報大,[5)]国立天文台

Exploring the roof of Jovian atmosphere by Subaru telescope including last day COMICS run

#Yasumasa Kasaba[1)], Hajime Kita[2)], Chihiro Tao[3)], Takeshi Sakanoi[1)], Takao M. Sato[4)], Takuya Fujiyoshi[5)], J.A. Sinclair[5)], Orton G.S.[5)]
[1)]Tohoku Univ.,[2)]Tohoku Inst. Tech.,[3)]NICT,[4)]HIU,[5)]NAOJ

Planet do not have their roofs. Their atmospheres are unstable area connected to outer space. This report introduces the two recent Subaru observations around this region on Jupiter, including the last day observations of COMICS (mid-IR imager and spectrometer) which open-use is terminated in July 2020.
(1) Emission from the thermosphere: Jupiter's intense magnetic field captures electrons and ions with orders of magnitude and energy higher than Earth. These enter into the thermosphere (altitude: ~200-1000s km), hit and heat the dilute atmosphere, producing strong aurora emissions. On the dayside seen from the earth, this emission is buried in the cloud reflection light. However, in UV and near IR light, the reflection light is suppressed by the CH4 absorption in the stratosphere (altitude: <~200 km), and thermospheric emission can be seen. In near IR, H3+ emission is evident. This emission was discovered by T. Oka and is bright in interstellar molecular clouds with energetic particles. Jovian thermosphere has a similar environment. The distribution of this emission was observed by Subaru/IRCS. Using Galilean satellites for AO188, we achieved the spatial resolution of ~250 km (0.1"). The strong emission spreads in an altitude of 500-1,000 km and the temperature reaches ~1,000 K or more. The atmosphere in higher altitude has a non-equilibrium state and is easier for escape. The spatial distribution was slightly strange. The H3+ emission is maximum in the UV aurora oval, which is consistent with H3+ molecule formations enhanced by energetic electrons. On the other hand, H2 emission fills the polar cap. This region is not bright in UV, but is known for X-ray emission by higher energy particles. This region is connected to the solar wind boundary region by a magnetic field, and the generation mechanism of high-energy particles here is one of the main targets of NASA Juno mission.
(2) Variation of hydrocarbons in the stratosphere, the mezzanine of Jupiter: High-energy particles that produce H2 emission in the polar cap can penetrate into the stratosphere. Up to this region, CH4 rises from the lower layer, and high-energy particles create more complex hydrocarbon molecules. These CxHy molecules have a lot of absorption and emission in the mid IR. The distribution and variations of these molecular emission was observed by Subaru/COMICS. Large sized aperture is important for the spatial decomposition. Other capability is only provided by the VLT. The stop of COMICS operation in July 2020 is disappointing. (We will be the final observer of this instrument.) In Jan and May 2017, we observed the distribution and variation of CH4 emissions covering the entire polar region as well as near IR H2 emission. It is shown that the precipitating high-energy particles can fluctuate the atmospheric temperature even in a short time scale, about one day, and progress to the production of complex hydrocarbons. It was also found that this fluctuation correlates with the solar wind pressure. It suggests that the influence of outer space can reach below than the thermosphere.

惑星に屋根はなく、その大気は宇宙空間へ地続きでつながる不安定な領域である。本稿は、太陽系最大の惑星・木星でこの領域を巡る直近の Subaru 観測成果２つを、共同利用が終了する中間赤外線観測器 COMICS による最終観測成果を含めて紹介する。
(1)木星の屋根裏、熱圏大気の発光を捉える：　木星は、巨大な磁場によって地球とは桁違いの量・エネルギーの電子・イオンを捉えている。これらが熱圏域(高度 200～数千 km)へ進入し、希薄大気を叩いて加熱し強力なオーロラ発光を生み出す。地球から見える昼間側では雲反射光に埋もれてこの発光は本来見えない。しかし、紫外・近赤外光では成層圏(高度約 200 km 以下)のメタン吸収によって雲反射光が抑制され、熱圏発光が顔を出す。近赤外では H3+ が明るく光る。この分子発光は岡武史先生により発見されたもので、高エネルギー粒子が降り注ぐ星間分子雲、そして似た環境にある木星熱圏を捉えるのに適する。この発光分布を Subaru/IRCS で捉えた。ガリレオ衛星を AO188 で捕捉し、空間分解能～250 km（0.1"）を達成した。高度 500～1,000 km に強発光域が広がり温度約 1,000 K 以上に達すること、より高高度では衝突減により非平衡状態となり、宇宙空間へ流出しやすいことを示した。やや不思議なのは空間分布である。H3+発光は、南北磁極をリング状に囲む紫外オーロラ域で最大となる。これは高エネルギー電子が H3+分子生成を引き起こすことと整合する。一方、H2 発光は極冠域を埋め尽くす分布となった。この領域は紫外線では暗いが、より高いエネルギーの粒子による X 線発光で知られる。この領域は太陽風境界域と磁場でつながっており、ここでの高エネルギー粒子の生成機構は木星周回中の NASA Juno 探査機の主観測テーマの１つである。
(2) 木星の中二階、成層圏大気の炭化水素の変動を捉える：　極冠域の H2 発光をもたらす高エネルギー粒子は成層圏まで進入しうる。ここまでは下層から CH4 が上昇し、高エネルギー粒子が衝突してより複雑な炭化水素分子を作り出す。これら CxHy 分子は中間赤外域で多くの吸収・発光をもつ。この分子発光の分布・変動を Subaru/COMICS

で捉えた。この空間分解には 8-m の大口径が重要である。同等の能力を持つ大口径鏡は他に欧 VLT しかなく、2020 年 7 月末の COMICS 停止は残念である（我々が最終観測者となった)。2017 年 1 月・2 月・5 月の観測では、近赤外 H2 発光と同様に極域全体を覆う CH4 等発光の分布と変動を捉えた。降下高エネルギー粒子が 1 日程度の短時間でも大気温度を変動させ、また複雑な炭化水素の生成へ進行させることを示す。この変動が太陽風圧と相関することも判明した。熱圏より深い高度まで宇宙空間の影響が及びうることを示唆する。2020 年 8 月以降、Subaru は中間赤外線観測能力を喪失するが、2022 年頃に稼働する東京大アタカマ 6.5-m 望遠鏡による観測能力実現に期待する。
本稿の主題である木星系では、NASA/Juno と JAXA/Hisaki 紫外線望遠鏡衛星が現主役で、2020-30 年代を目指して NASA/Europa Clipper、ESA/JUICE が開発中である。私たちは Hisaki 開発に参加し、JUICE 観測装置の開発中でもある。とはいえ、惑星探査機群は重量制約が厳しく万能観測手段ではない。地球からの望遠鏡観測はより地味ではあるが、より継続的な観測によってこれらを支える。また、JAXA-ESA で開発途上にある赤外線天文衛星 SPICA、そして Hisaki 紫外線極端紫外線望遠鏡衛星の後継機開発にも参加貢献し、戦力増大を図る。

R009-08
Zoom meeting D ：11/1　AM2　(10:45-12:30)
11:15-11:30

Euler potential を用いた木星磁気圏磁場モデル

#桃木　尚哉[1)],藤　浩明[2)]
[1)]京都大学・大学院・理学・地惑,[2)]京都大学・大学院・理学・地磁気センター

Magnetic field models of Jovian magnetosphere using Euler potentials

#Naoya Momoki[1)], Hiroaki Toh[2)]
[1)]Earth and Planetary Sciences, Kyoto Univ.,[2)]DACGSM, Kyoto Univ.

Since the first observation by Pioneer 10 in 1973, observations around Jupiter have been carried out by several spacecrafts up to the currently operating Juno, and thus magnetic field data have also accumulated. One of the main researches on them is the magnetic field modeling in and around Jupiter, which is divided into the Jovian intrinsic and magnetospheric field models.

Many magnetospheric field models have followed a procedure in which current systems are placed within the magnetosphere or on the magnetopause. The current sheet is considered as a typical current system of the former. The model by Connerney et al. [1981] is a good example in the early stage, and the magnetospheric field was calculated assuming a current sheet in the azimuthal plane on the Jovigraphical equatorial plane. There are also many studies on the shape of the current sheet such as Goertz [1981] and Khurana and Schwarlz [2005], and it eventually became a consensus that the current sheet changes its shape due to the tilt of the magnetic dipole, the delay from Jovian co-rotation, and the solar wind.

In this study, we adopted the formulation by Khurana [1997] as a magnetic field modeling method, and redetermined the Jovian magnetospheric field model including the data by Galileo and Juno obtained after the publication of Khurana [1997].

The adopted modeling method consists of two steps: (1) approximation of the current sheet by a hinge model, and (2) construction of the magnetospheric model by the Euler potentials. (1) was adopted by Khurana [1992]. The current sheet was assumed perpendicular to the magnetic dipole in the vicinity of Jupiter, and perpendicular to Jupiter's rotation axis when it is away from Jupiter in the anti-sun direction. It also included the delay of the co-rotation of both plasma and current sheet caused by the radial movement of the plasma. When a spacecraft crosses the current sheet, the radial magnetic component is expected to be zero. So, we first estimated crossing points using the observed data. Then, 3 parameters of the hinge model were determined by a least square method to give the best fit to the observed crossing points. (2) is the modeling method adopted by Khurana [1997], in which the hinged current sheet model by Khurana [1992] is included. The magnetospheric field itself was formulated using two Euler potentials.

Since the magnetic field vector, $\mathbf{B}$, is solenoidal, it can be expressed by two scalar functions. $\mathbf{B}$ can be expressed in the form of $\nabla f * \nabla g$ by setting the magnetic vector potential, $\mathbf{A}$, as $f\nabla g$ where f and g are the Euler scaler potentials. The magnetic field lines satisfy f=const. and g=const. The first Jovian magnetic field model using the Euler potentials appeared in Goertz et al. [1976], which became a prototype of the Khurana's [1997] model. In their model, both intrinsic and magnetospheric magnetic fields were expressed by the Euler potentials. In Khurana [1997], however, only the magnetospheric field was expressed by the Euler potentials, and an existing model was adopted for the intrinsic field. In this study, we also adopted the latest model of Jupiter's intrinsic field by Connerney et al. [2018], i.e., JRM09.

Specifically, since the observed data can be considered as a sum of the intrinsic and magnetospheric fields, we subtracted JRM09 from the observed data in advance, and defined the residual as the observed magnetospheric field. Using the residuals, 14 model parameters of the two Euler potentials were determined by another least square method.

In the presentation, we will also argue comparison of averaged magnetospheric field models for each of the three legendary periods, viz., pre-Galileo, Galileo and Juno to confirm whether there are secular changes in the Jovian magnetospheric field in nearly half a century from Pioneer 10 to Juno. We will further discuss whether seasonal changes (w.r.t. orbital positions of Jupiter) and changes due to solar activities during each period exist or not.

木星圏では，1973 年に Pioneer10 による初観測以来,現在運用中の Juno に至るまで幾つかの探査機による観測が行われ,磁場データが蓄積されてきた。これらの磁場データを用いた主な研究成果の一つに木星圏の磁場モデリングがあり,それらは木星固有磁場モデルと磁気圏磁場モデルの二つに大別される。

磁気圏磁場モデルは，磁気圏内または圏界面上に電流系を置いて磁気圏磁場を計算するという手順のものが多く,カレントシートが代表的な電流系として議論される。Connerney et al. [1981]によるモデルが初期における典型例であり,木星の地理的赤道面上を方位角方向に流れるカレントシートを仮定し,磁気圏磁場の計算を行っている。また,Goertz [1981]や Khurana and Schwarlz [2005]などカレントシートの形状に関する研究も多く存在し,カレントシートは磁気双極子の傾き,木星共回転からの遅れ,太陽風などによる影響により時間変化するものとして捉えられるようになった。

そこで本研究では，磁場のモデリング手法として, Khurana [1992]によるカレントシートモデルに Euler potential を組み合わせた Khurana [1997]の定式化を採用し,この論文の発表後に取得された Galileo と Juno のデータを含めて木星磁気圏磁場モデルを再決定した。

採用したモデリング手法は, (1)カレントシートの蝶番モデルによる近似, (2)Euler potential による磁気圏モデルの構築,の二段階からなる。(1)は Khurana [1992]で採用されたものであり，カレントシートは木星の近傍で磁気双極子に垂直に,木星から反太陽方向へ離れると木星の自転軸に垂直(おおよそ太陽風に平行)になると仮定している。また，プラズマが動径方向へ移動することによって起こるプラズマ及びカレントシートの木星共回転からの遅れも含んでいる。探査機がカレントシートを通過する際には，磁場の動径方向成分が零となることが予想され,観測データから得られた動径方向成分の零点(シート通過点)と，モデルから計算されるシート通過点が最も良く合う 3 個のモデルパラメータを最小二乗法により決定した。(2)は Khurana [1997]において採用された磁場モデル法で,モデル中に Khurana [1992]によるカレントシートモデルを既知のものとして含め，二つの Euler potential を用いて磁気圏磁場を計算した。

磁場ベクトル $\mathbf{B}$ は,非発散であることから二つのスカラー関数を用いて表現することができる。磁場ベクトル $\mathbf{B}=\nabla\times\mathbf{A}$ を与えるベクトルポテンシャル $\mathbf{A}$ を二つのスカラー関数 f, g を用いて $\mathbf{A}=f\nabla g$ と置くことにより,磁場ベクトルは $\mathbf{B}=\nabla f\times\nabla g$ という形に表現できる。この f, g を Euler potential と呼び,磁力線は f=const.かつ g=const.を満たす。Euler potential を用いた他の木星磁場モデルとしては, Khurana [1997]モデルの原型である Goertz et al. [1976]が挙げられる。Goertz 他のモデルでは，固有磁場と磁気圏磁場はどちらも Euler potential を用いて表現されたが, Khurana [1997]では磁気圏磁場モデルのみを Euler potential で表現し,固有磁場については既存のモ　デルが採用された。特に本研究では，　Connerney et al. [2018]による最新の木星固有磁場モデルを採用することとした。

具体的には，元データは，固有磁場と磁気圏磁場の和であると考えられるので，元データから Connerney et al. [2018]による木星固有磁場モデルをあらかじめ差し引き,残差を外部電流系による磁場,すなわち磁気圏磁場モデルに対応する観測磁場であると定義した。この残差を用いて Euler potential を表す 14 個のモデルパラメータを最小二乗法により決定した。

本講演ではさらに, pre-Galileo, Galileo, Juno の 3 期間それぞれにおいて平均的な磁気圏磁場モデルパラメータを求め,それらの比較から Pioneer10 から Juno に至る半世紀近いデータの蓄積により得られた木星磁気圏磁場に,経年変化が存在するかどうかも併せて議論する。加えて,各期間中に季節変化（木星の公転軌道位置）や太陽活動度による変化があるかどうかについても議論する。

R009-09
Zoom meeting D ：11/1　AM2　(10:45-12:30)
11:30-11:45

ひさき衛星観測との比較を目指した木星内部磁気圏プラズマ動径方向拡散モデルの開発

#山口　和輝[1)2)],土屋　史紀[1)2)],坂野井　健[1)2)],鍵谷　将人[1)2)],加藤　雄人[2)],川面　洋平[2)],木村　智樹[2)],古賀　亮一[3)],吉岡　和夫[4)],疋田　伶奈[5)]
[1)]東北大・理・惑星プラズマ大気研究センター,[2)]東北大・理・地球物理,[3)]名古屋大・環境学研究科・地球環境科学専攻,[4)]東大・新領域,[5)]東大・理・地惑

Radial diffusion model of Jovian inner magnetospheric plasma with HISAKI observation

#Kazuki Yamaguchi[1),2)], Fuminori Tsuchiya[1),2)], Takeshi Sakanoi[1),2)], Masato Kagitani[1),2)], Yuto Katoh[2)], Youhei Kawazura[2)], Tomoki Kimura[2)], Ryoichi Koga[3)], Kazuo Yoshioka[4)], Reina Hikida[5)]
[1)]PPARC, Tohoku Univ.,[2)]Dept. Geophys., Grad. Sch. Sci., Tohoku Univ.,[3)]Dept. Earth and Planetary Scicences, Grad. Sch. Environmental Studies, Nagoya Univ.,[4)]The Univ. of Tokyo,[5)]the Univ. of Tokyo

We developed a time-dependent radial diffusion model to evaluate chemical reactions and radial transport of ions and electron in the Jovian inner magnetosphere. We compared equilibrium plasma distribution with the HISAKI observation to validate the model, then investigated mass and energy flows in the magnetosphere when plasma source from Io temporally changed.
Jovian first satellite Io has lots of active volcanoes and SO_2 rich atmosphere [Pearl et al., 1979; Fanale et al., 1979] and supplies ~tons/s of neutral gases to the magnetosphere. The gases are ionized and picked up by magnetic field, and distribute in a donut shape called Io Plasma Torus (IPT). About 90% of total mass of the magnetospheric plasma is supplied from IPT [Hill, Dessler, and Goertz, 1983]. The plasma diffuses outward on the time scale of several tens of days while obtaining the rotation angular momentum of Jupiter. Revealing the mass and energy balance of plasmas is an important subject to understand the macroscopic physical phenomena in the Jovian inner magnetosphere.
The radial distribution of the plasma has been examined based on steady state models and observations of Voyage 1, 2 and Cassini spacecraft. However, the time dependent model and comparison of the model with continuous observations have not been reported yet. The purpose of this study is to develop a model that has a capability to track the time variation of the radial distribution and compare it with HISAKI observation.
In the model, we track mass and energy balances of major heavy ions of Io origin (O^+-O^{3+} and S^+-S^{4+}). The equation system is based on the mass and energy transport model (Delamere et al. 2005). The radial gradient of the density and temperature were set to 0 at the inner boundary (Io's orbit, 5.9 R_J from Jupiter), and they are fixed with extrapolated values of HISAKI observation at the outer boundary (30R_J). We considered several chemical interactions: charge exchange, electron impact ionization, electron recombination, Coulomb interaction and radiation through electron collision excitation (Delamere & Bagenal 2003). The initial values of temperature and density of ions and thermal electrons were given from the HISAKI observations in November 2013 when Io's volcanic activity was stable [Yoshioka et al. 2018]. The density of neutral atoms (O, S) were also given by HISAKI observation [Koga et al. 2018] as initial values, and their total source rate is a free parameter. To express the radial diffusion physically realistic, we adopted the diffusion coefficient $D_{LL} = -k_\Omega L^{p+4}(dNL^2/dL)$ driven by the interchange instability in Jovian inner magnetosphere [Siscoe & Summers 1981].
In order to verify the validity of the model, the steady state temperature and density of ions and electrons in the region of 6-10 R_J were compared with the HISAKI observation and we tried to get the parameters that best matched with the observation.
Electron temperature and density of the lower charged ions and electron are almost matched the HISAKI observation. However, we found that highly ionized ions have low density with HISAKI, and ion temperature is almost stable around 200 eV except S^+ which has 300 eV. Under this condition, we obtained three parameters: the hot electron fraction is 0.3 (%), the neutral source rate is 7.0×10^{-4} ($/m^3/s$), and k_Ω is estimated to be 1.2×10^{-19} near Io's orbit. The source rate and hot electron fraction is consistent with the Cassini observation. k_Ω is also consistent with the theoretical estimation: 6.2×10^{-20} to 7.8×10^{-18}.
As for the time variations of density and temperature, we compared our model with the previous model with static radial diffusion coefficient.
In our model, diffusion increases during the volcanic event because the diffusion coefficient depends on the gradient of density and the radial profiles return to the equilibrium status after the event faster than the static radial diffusion model. In this presentation, we will show the correspondence between the mass/energy balance in the time variations and the HISAKI observation results.

R009-10
Zoom meeting D ：11/1 AM2 (10:45-12:30)
11:45-12:00

Numerical simulation of the passive subsurface radar for Jupiter's icy moons

#Tomoki Kimura[1)], Atsushi Kumamoto[2)], Fuminori Tsuchiya[3)], Yasumasa Kasaba[3)]
[1)]FRIS, Tohoku University,[2)]Dept. Geophys, Tohoku Univ.,[3)]Planet. Plasma Atmos. Res. Cent., Tohoku Univ.

The subsurface ocean at icy bodies in our solar system is one of the most likely habitable environments except for Earth. While the subsurface ocean of Enceladus at Saturn has been already demonstrated with the Cassini explorer, it is still unclear that Europa and Ganymede at Jupiter have it although they are theoretically predicted to have greater amount of liquid water than Earth. The highest priority is placed on detections of the subsurface ocean and related water plume activities at Jupiter's icy moons in the Jupiter Icy Moon Exploration mission JUICE, which is going to start exploration in early 2030s. Here we numerically simulate the passive subsurface radar PSSR for the icy moon's ocean that is going to be observationally made by receiving Jupiter's auroral radio emissions with the radio and plasma wave instrument RPWI onboard JUICE. Based on the ray tracing method, we simulate propagation of Jupiter's radio emission in the icy moon's water plume, tenuous ionosphere, and interior assuming the plasma density and dielectric constant structures. The simulation indicated that some of the structures are clearly detectable by PSSR if the incident radio emission forms chirpy waveform packets at HF frequencies. In this presentation, we are going to report some more simulation results under more realistic conditions.

R009-11
Zoom meeting D ：11/1　AM2　(10:45-12:30)
12:00-12:15

地上望遠鏡を用いた木星氷衛星における非 H_2O 氷の探索

#高木　聖子[1)],松尾　太郎[2)],木村　淳[3)]
[1)]北海道大学,[2)]名古屋大学,[3)]大阪大学

A search for the non-water ices on the Galilean moons of Jupiter with Pirka telescope

#Seiko Takagi[1)], Taro Matsuo[2)], Jun Kimura[3)]
[1)]Hokkaido Univ.,[2)]Nagoya University,[3)]Osaka University

In the outer region of the Solar System, the Jovian system and beyond, most of solid bodies are generally covered with the solid water ice on their surfaces, and thus they are called as icy bodies. In addition, various non-water ice(s) can be found on the many objects, e.g., CH_4 and NH_3 in the Saturn moons and N_2 and CO in the Neptunian moon Triton and the icy dwarf planet Pluto. In the Jovian system, the only non-water volatiles which have been inferred is CO_2, by the presence of an absorption band at ~4.26 microns in reflectance spectra returned by the Near Infrared Mapping Spectrometer (NIMS) onboard the Galileo spacecraft. On Callisto, trailing hemisphere and several fresh impact craters show enrichment in carbon dioxide. On the other hand, no such distributions of CO_2 can be seen on Ganymede. Thus the origin of CO_2 on their moons, whether these are primordial and degassed from the interior or are exogenic and delivered through the impact, is still controversial. As a first approximation, highly volatile ices exist in a farther region from the Sun, identifying the presence of non-water ices on the Jovian system could be an important key to know the temperature environment during the formation of the solar system and the position of each planetary system.
We search the non-water ices (CH_4 and NH_3) on the Galilean moons of Jupiter using the ground-based telescope of Hokkaido University (Pirka telescope, the primary mirror is 1.6-m in effective diameter). The Pirka telescope and its onboard instrument has started full-scale operation in 2011 with priority to observe planetary bodies in the Solar System. The visible multi-spectral imager (MSI) has been mounted at the Cassegrain focus of the telescope and it allow us to obtain surface spectral data of Galilean moons of Jupiter at wavelength between 540 and 940 nm. Here we will report the investigation.

太陽系の巨大惑星やそれ以遠の領域にある固体天体はあまねく、その表面が固体 H_2O を主体とした氷で覆われており、氷天体と呼ばれる。氷天体には、固体 H_2O 以外の氷が共存するものも多い。例えば土星系の衛星エンセラダスには CH_4 や NH_3 が存在し、海王星系の衛星トリトンや冥王星では N_2 や CO の氷なども見られる。対して、木星系の氷衛星ではその兆候が乏しい。ガリレオ探査機に搭載された近赤外分光計 NIMS の観測によれば、ガニメデやカリストにおいて CO_2 の存在が示唆されているものの、その起源（内因性か外部由来か）は定かではない。これらの様々な揮発性物質は、第一近似的には揮発性の高い物質ほど太陽から遠い天体に存在しているように見えることから、それらの分布を知ることは太陽系形成時の温度環境や各惑星系が形成した位置などを探る鍵になるかもしれない。
北海道大学大学院理学研究院附属天文台（北緯 44.4°、東経 142.5°）は北海道名寄市にあり、地上望遠鏡（ピリカ望遠鏡）を所有している。ピリカ望遠鏡とその搭載観測装置は、惑星を優先的に観測することを目的として 2011 年に本格運用を開始した。主鏡口径は 1.6 m であり、その大きさは惑星観測用の望遠鏡としては世界最大級である。ピリカ望遠鏡のカセグレン焦点には、本研究院宇宙惑星グループによって開発されたスペクトル撮像装置 MSI（350～1050 nm）が搭載されている。我々は木星系における非 H_2O 氷の有無に焦点を当て、2018 年からガリレオ衛星観測（540～940 nm）を継続している。本発表では非 H_2O 氷の捜査報告を行う。

R009-12
Zoom meeting D ：11/1　PM1　(13:45-15:30)
13:45-14:00

広域・高時間分解観測から迫る空電と雷雨に関連した木星雷由来の電波パルス

#今井　雅文[1)],Michael　Wong[2)3)],Kolmasova　Ivana[4)],Brown　Shannon[5)],Santolik　Ondrej[4)],Kurth　William[6)],Hospodarsky　George[6)],Bolton　Scott[7)],Levin　Steven[5)]
[1)]新居浜高専,[2)]SETI Institute,[3)]Center for Integrative Planetary Science, University of California, Berkeley,[4)]The Czech Academy of Sciences,[5)]Jet Propulsion Laboratory, California Institute of Technology,[6)]University of Iowa,[7)]Southwest Research Institute, San Antonio

High-Spatiotemporal Resolution Observations of Jupiter Lightning-Induced Radio Pulses Associated With Sferics and Thunderstorms

#Masafumi Imai[1)], Michael H. Wong[2),3)], Ivana Kolmasova[4)], Shannon T. Brown[5)], Ondrej Santolik[4)], William S. Kurth[6)], George B. Hospodarsky[6)], Scott J. Bolton[7)], Steven M. Levin[5)]
[1)]National Institute of Technology, Niihama College,[2)]SETI Institute,[3)]Center for Integrative Planetary Science, University of California, Berkeley,[4)]The Czech Academy of Sciences,[5)]Jet Propulsion Laboratory, California Institute of Technology,[6)]University of Iowa,[7)]Southwest Research Institute, San Antonio

Since 5 July 2016, the Juno spacecraft has been in polar orbit around Jupiter. During Juno perijoves every 53 days, synoptic observations of lightning at radio wavelengths are made by the radio and plasma wave instrument (Waves) and by the Microwave Radiometer (MWR). Constraints from operational modes and geometrical considerations mean that the two instruments rarely achieve truly simultaneous coverage. The reception of lightning-induced radio waves is dependent on the topology of Jupiter's magnetic field lines for Jovian whistlers and on the orientation of the spacecraft spin plane with respect to the planet's atmosphere for UHF sferics detected by the MWR. Here we investigate quasi-simultaneous Waves and MWR data acquired around noon UTC on 6 April 2019. During this pass, Juno's on-board imaging instruments were shutdown to accommodate an MWR cross-track scanning orientation, so we use Hubble Space Telescope (HST) imaging for atmospheric context.
On 6 April 2019, the Juno Waves instrument captured an extraordinary series of radio pulses at frequencies below 150 kHz on timescales of submilliseconds. Quasi-simultaneous multi-instrument data show that the locations of their magnetic footprints are very close to the locations of UHF sferics recorded by the Juno MWR instrument. HST images show that the signature of active convection includes cloud-free clearings, in addition to the convective towers and deep water clouds that were also recognized in previous spacecraft observations of lightning source regions. Furthermore, the detections of 17 VLF/LF radio pulses suggest a minimum duration of lightning processes on the order of submilliseconds. These observations provide new constraints on the physical properties of Jupiter lightning.

2016 年 7 月 5 日に NASA の Juno 探査機が木星極周回軌道に投入されて以来、極軌道でしか見ることができない木星雷のユニークな観測が行われてきた。53 地球日毎に探査機は木星に最接近し、波動観測装置（Waves）とマイクロ波放射計（MWR）によって、木星雷由来の電波を観測している。機器の観測モードや幾何学的位置関係による制限は二つの独立した観測装置が同時及び同じ領域を向いていることは非常に稀であることを意味する。雷由来の電波観測は、ホイッスラー波に関して、木星磁力線の形状に依存し、UHF 帯空電に関して、惑星の大気と探査機のスピン面との幾何学的な位置に依存する。本研究では、2019 年 4 月 6 日正午 UTC 頃に Waves と MWR 両機器が観測したデータを解析する。解析期間中は Juno 探査機が MWR クロストラック姿勢を行う関係で、同探査機に搭載された全ての光学カメラの電源はシャットダウンされていた。そのため、ハッブル宇宙望遠鏡（HST）で得られた木星大気データを併用する。
2019 年 4 月 6 日に Waves がサブミリ秒オーダーで変動する稀な電波パルス群（周波数<150kHz）を観測した。準同時多地点観測データより、それらの磁力線の麓は MWR が観測した UHF 帯空電の電波源の近くであることが示された。さらに、HST の木星大気観測から、従来の衛星観測で知られる対流雲及び深い水雲に加え、新たに雲の無い空間が雷現象と密接に関連していることを示唆した。一方、VLF/LF 帯電波パルスの検出は雷放電がサブミリ秒以下のタイムスケールで発達することを意味する。Juno 探査機と HST を組み合わせた多地点観測より、木星雷の物理過程を解明するための新たな制約を与えた。

R009-13
Zoom meeting D ：11/1　PM1　(13:45-15:30)
14:00-14:15

地上望遠鏡と光電子倍増管を利用した惑星雷発光の観測

#大野　辰遼[1)],高橋　幸弘[2)],佐藤　光輝[3)],渡部　重十[2)],高木　聖子[1)],今井　正尭[4)]
[1)]北海道大学,[2)]北大・理・宇宙,[3)]北大・理,[4)]産総研

Planetary lightning flashes observation using ground based telescope with Photomultiplier tube

#Tatsuharu Ono[1)], Yukihiro Takahashi[2)], Mitsuteru SATO[3)], Shigeto Watanabe[2)], Seiko Takagi[1)], Masataka Imai[4)]
[1)]Hokkaido Univ.,[2)]Cosmosciences, Hokkaido Univ.,[3)]Hokkaido Univ.,[4)]AIST

Lightning in planetary atmospheres is generated by the convections. The detection of lightning can be used to understand the atmospheric dynamics and the large-scale structures on other planets. In the case of Jupiter, the lightning flashes have been observed. Previous studies (e.g. Gierasch et al., 2000; Ingersoll et al., 2000) suggested that zonal jet is driven by the merging of small-scale eddies that receive their energy from moist vertical convection which similar to thunderstorm on the Earth. Although it is difficult to observe the vertical convections within the dense clouds, lightning is correlated with the cumulonimbus, and thus lightning observations can be used to investigate the formation of Jupiter's zonal jet. In Venus, the existence of Venusian lightning is controversial for 40 years. The possible generation mechanisms are convection, volcanic, or aeolian triboelectric activity. In the previous study, there are radio wave observations and optical observations with CCD. Although some of the observations have detected lightning, no unambiguous lightning flash events have been detected by LAC (Lightning and Airglow Camera) onboard AKATSUKI Venus Climate orbiter (Lorenz et al., 2019). There is no robust evidence of existence the lightning because it is difficult to distinguish between the lightning signal and the electrical noise or other plasma waves, the observation area is limited, and the CCD's sensitivity is not enough to detect the lightning. If we can confirm the existence of Venusian lightning like the Jovian, it could also be useful as an indicator of Venusian atmospheric dynamics.
To reveal the relationship between lightning and atmospheric dynamics of Jupiter and Venus, we have developed the Planetary Lightning Detector (PLD), which is the high-speed and high-sensitive lightning detector mounted on a 1.6-m ground-based telescope by using a photomultiplier tube to observe the planetary lightning flashes. Using this telescope we can get an observation period at least one hour per day for several months, longer than the previous studies. We can obtain the light-curve of flash events with a sampling rate of >20 s^{-1} to distinguish the other flashes and decrease the contamination of dayside light and sky background to improve the Signal-to-Noise ratio. We will reveal the distribution of lightning and its frequency, and then we derive the distribution of a few tens km scale vertical convections. We compare the results and the variation of wind velocity and cloud distribution to reveal the atmosphere dynamics.
777.4 nm is the strongest emission line in the Venus lightning spectra (Borucki et al. 1996). PLD equips narrowband filter (FWHM = 1 nm) of 777 nm. PLD observes the light curve by using a photomultiplier tube. The minimum exposure time is 50 microseconds. The maximum time resolution is about $2x10^4$ points/s. The FOV of PLD can be changed to 5", 10", 30", 60" pinhole, and 2"x11" slit by using field stops. The slit or pinhole is used for Venus's night-side observation. To obtain the lightning's light curve, we operate the bandpass filter or other signal process to remove the shot noise and large time scale variation by Earth's atmosphere. We have observed Venus and Jupiter by using PLD from May 2020. In our Venus observation, we could find several possible lightning events having large count values above 4-sigma of the background level from the May data. The number of the detected event is 3 events per 2000 s observation period. The estimated peak energy of light-curve is about 10^8 J. The calculated rate of flash event is about 10^{-11} [$s^{-1}km^{-2}$]. It is ten times larger than the rate of previous study $2.7x10^{-12}$ [$s^{-1}km^{-2}$] (Hansell et al., 1995). Although, our observation duration is not enough to compare with the previous study. we will increase the total observation time more than 3 hours.
In this time, we will introduce the developed lightning observation instrument PLD and present our observation results obtained from May 2020. We will also show our future coordinated observation with LAC.

R009-14
Zoom meeting D ：11/1 PM1 (13:45-15:30)
14:15-14:30

Signal recorded by LAC onboard Akatsuki

#Yukihiro Takahashi[1)], Masataka Imai[2)], Mitsuteru SATO[3)], Tatsuharu Ohno[4)], Ralph D. Lorenz[5)]
[1)]Faculty of Science,Hokkaido Univ.,[2)]AIST,[3)]Hokkaido Univ.,[4)]Cosmosciences, Hokkaido Univ.,[5)]Applied Physics Laboratory, Johns Hopkins University

The existence of lightning discharge in Venus has been controversial well over three decades, which might be attributed to the lack of conclusive observational evidence. There had been no satellite payload intentionally designed for the detection of lightning phenomena using radio wave or optical sensors. LAC, lightning and airglow camera, onboard Akatsuki spacecraft, is the first sensor optimized for the lightning optical flash measurement in planets other than the Earth. The unique performance of LAC compared to other equipment used in the previous exploration of Venus is the high-speed sampling rate at 20 kHz with 32 pixels of Avalanche Photo Diode (APD) matrix, enabling us to distinguish the natural optical lightning flash from other pulsing noises, including artificial electrical noise and cosmic rays. We selected OI 777 nm line for lightning detection, which is expected to be the most prominent emission in the CO2-dominant atmosphere based on the laboratory experiments.
? ? We have been conducting a lightning search in about 40 passes of AKATSUKI with triggering parameter set optimized for the light curve similar to the normal lightning and also sprite type in the Earth. On March 1, 2020, LAC recorded a signal, which seems like a kind of optical flash. The total coverage of the LAC lightning hunt is now about 100 [million km2-hr]. If the flash is from lightning discharge, the occurrence rate could be equivalent to that with a ground-based telescope reported by Hansell et al. (1995). On the other hand, we are examining the possibility of bolide carefully. If it's bolide, the magnitude observed on the ground might be 10 times brighter than a full moon in the earth.

R009-15
Zoom meeting D ：11/1　PM1　(13:45-15:30)
14:30-14:45

あかつき IR2 による金星夜面データから発見された静穏雲領域

#佐藤　毅彦[1)3)],佐藤　隆雄[2)],Vun　Choon Wei[3)],堀之内　武[4)]
[1)]宇宙研,[2)]情報大,[3)]SOKENDAI,[4)]北大・地球環境

Quiescent cloud regions in Venus night-side discovered by Akatsuki/IR2

#Takehiko Satoh[1),3)], Takao M. Sato[2)], Anthony Vun[3)], Takeshi Horinouchi[4)]
[1)]ISAS, JAXA,[2)]HIU,[3)]Space Sciences, SOKENDAI,[4)]Hokkaido University

We have analyzed the Venus night-side data acquired by Akatsuki/IR2 (2.26um and 1.735um) after cleaning of contamination from the day crescent by the RSS (Restoration by Simple Subtraction) method. Could regions which seem to be especially quiescent were discovered. The coordinate system, with the radiance at 2.3um as horizontal axis and the radiance at 1.74um as vertical axis (both are logarithmic), has been widely used after Carlson et al. (1993) who analyzed the Galileo/NIMS data. We have introduced a new coordinate system, named "M3L", by modifying the vertical axis to $\log(I_{1.735um})$-0.519*$\log(I_{2.26um})$, enabling effective discrimination of aerosol sizes. A prominent cluster of data, named CALM, was found to be corresponding to the bright mid-latitude regions once remapped to the images. Interestingly, brightest regions, such as the boundary with darker equatorial region, or bright mid-to-high latitude streaks are excluded from CALM. Therefore, CALM is interpreted as very quiescent regions in which gentle convection causes particle size changes in an ordered manner (governed by equilibrium of aerosols and sulfuric acid vapor). On the other hand, brightest regions may be with forced down-welling in which particles evaporate rapidly, resulting in deviations from CALM. This discovery successfully demonstrates adequateness of the RSS method, quality of the restored IR2 data, and effectiveness of the new M3L coordinate system.

RSS（Restoration by Simple Subtraction）法により昼面からのコンタミを除去したあかつき IR2 金星夜面データ（2.26um, 1.735um）を解析して、特に「静穏」と思われる雲領域を発見した。Galileo/NIMS データを解析した Carlson et al.(1993)以来、横軸に 2.3um 輝度、縦軸に 1.74um 輝度（いずれも対数）をとったプロットがしばしば使われる。本研究では縦軸を log(1.735um 輝度)-0.519*log(2.3um 輝度)とした新座標系（M3L と命名）を導入し、雲粒子のサイズ比率識別を容易とした。この中で特に集中したデータ点を金星画像に再マップすると、中緯度に見られる比較的明るい（雲があまり濃くない）領域に対応することが分かり、CALM と名づけた。そうした明るい領域であっても、たとえば暗い赤道域との境界で特に明るい部分や、あるいは中～高緯度に見られる明るいストリークは CALM に含まれないことも分かった。つまり、CALM 領域においてはマイルドな対流の中で粒子サイズが一定の範囲内を規則的に変化（周囲の硫酸蒸気との平衡を保ちつつ）していると予想され、特に明るい領域は強制的な下降気流が引き起こす急速な蒸発による粒子サイズ変化が CALM からの逸脱をもたらすのであろう。このような静穏雲領域の識別は初めてのことであり、RSS 法による IR2 データ補正の威力、新 M3F 座標系の有効性を示すことができた。

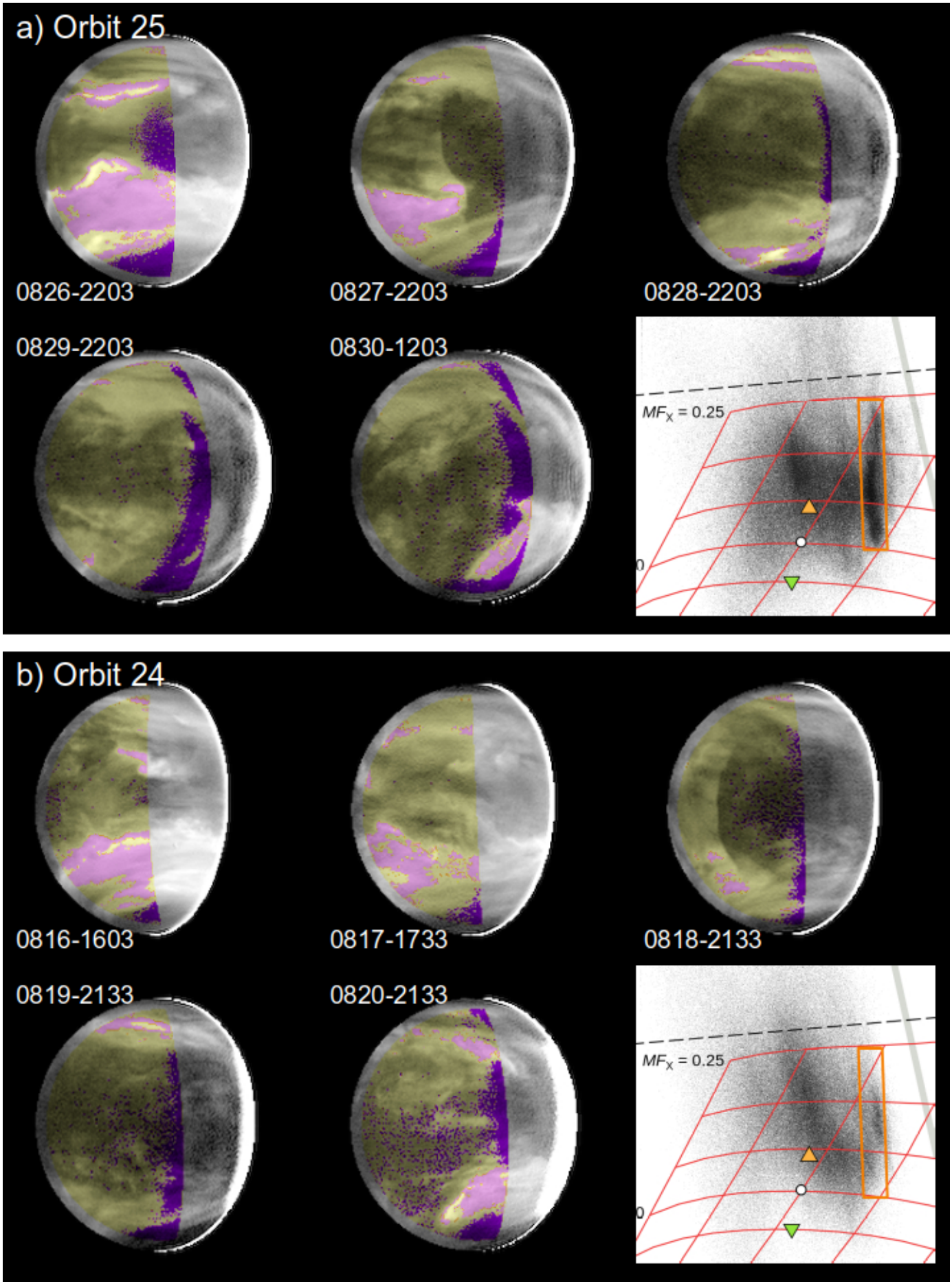
a) Orbit 25
0826-2203
0827-2203
0828-2203
0829-2203
0830-1203
MF_X = 0.25
0
b) Orbit 24
0816-1603
0817-1733
0818-2133
0819-2133
0820-2133
MF_X = 0.25
0

R009-16
Zoom meeting D ：11/1　PM1　(13:45-15:30)
14:45-15:00

金星の上層大気で観測された気温擾乱と AFES-Venus による比較

#尾沼　日奈子[1)],野口　克行[2)],杉本　憲彦[3)],高木　征弘[4)],安藤　紘基[5)],今村　剛[6)]
[1)]奈良女大・理・環境,[2)]奈良女大・理・環境,[3)]慶大・日吉物理,[4)]京産大・理,[5)]京産大・理,[6)]東京大学

Temperature fluctuations observed in the Venus upper atmosphere and its comparison with simulation by AFES

#Hinako Onuma[1)], Katsuyuki Noguchi[2)], Norihiko Sugimoto[3)], Masahiro Takagi[4)], Hiroki Ando[5)], Takeshi Imamura[6)]
[1)]Nara Women's Univ.,[2)]Nara Women's Univ.,[3)]Physics, Keio Univ.,[4)]Faculty of Science, Kyoto Sangyo University,[5)]Faculty of Science, Kyoto Sangyo University,[6)]The University of Tokyo

We detected large amplitude of temperature fluctuations in the upper atmosphere of Venus (75-90 km) by the Akatsuki radio occultation measurements. The vertical wave lengths of the observed temperature fluctuations are considerably shorter than the one of thermal tides expected to exist. We expect that atmospheric gravity waves cause the observed temperature fluctuations in those altitude ranges. A general circulation model for the Venus based on the AFES (AGCM for Erath Simulator), which has a high spatial resolution and can directly simulate gravity waves, reproduced temperature fluctuations similar to the observed ones. The temperature fluctuations distinctively appeared when we included thermal tides in the model, which suggests the relation of the observed temperature fluctuations to thermal tides.

金星探査機「あかつき」で実施された電波掩蔽観測では、高度 75～90km 付近において大きな振幅（数 K 程度）をもつ気温擾乱が見られた。この気温擾乱の振幅は、考え得る測定誤差よりも大きい。過去の研究ではこのような大きな振幅を持つ気温擾乱が熱潮汐波に関連するという示唆があるものの、観測された気温擾乱の鉛直波長は 2～3km 以下であり熱潮汐波そのものであるとは考えにくい。
我々は、この気温擾乱が大気重力波によるものではないかという予想のもと、大気重力波を解像可能なほどの高空間分解能を持つ金星大気大循環モデル AFES-Venus を用いた研究を進めている。モデルにおいて熱潮汐波が発生するような条件設定にすると（つまり、太陽による雲層の加熱の経度依存性を考慮すると）、着目している高度域で気温擾乱が大きくなることが示された。熱潮汐波の東西波数 2 ないし 3 の構造に沿って、気温擾乱も顕著であった。このことに加え、AFES は対流を直接計算していないことから、モデルにおける気温擾乱の発生は雲層における対流起因ではなく熱潮汐波が関与していることが推測できる。講演では、大気安定度やシア不安定との関連性についても議論する。

R009-17
Zoom meeting D ：11/1 PM1 (13:45-15:30)
15:00-15:15

Initial results of HCl abundance at the cloud top of Venus retrieved from IRTF/iSHELL spectra

#Takao M. Sato[1)], Hideo Sagawa[2)]
[1)]Hokkaido Information University,[2)]Kyoto Sangyo University

The atmosphere of Venus can be divided into three altitudinal regions with different chemical conditions. High temperature and pressure and the absence of effective photolysis processes are dominant in the lower atmosphere up to 60 km where solar radiation longer than UV can reach. The middle atmosphere between 60 and 110 km is controlled by photochemistry driven by solar UV radiation. In the upper atmosphere above 110 km, dissociation, ionization, and ionospheric reactions are important processes.
HCl is the primary chlorine reservoir in the Venus atmosphere bellow 110 km. Highly reactive chlorine species (ClO_x) is produced by solar UV photolysis of HCl and has been proposed to play an important role in catalysis of CO and O recombination to CO_2, thereby stabilizing the CO_2 atmosphere. Chlorine chemistry is also linked to sulfur chemistry and its understanding is necessary to explain the observed vertical distribution of SO_2.
Interestingly, there is a large inconsistency between the HCl abundances measured by spacecraft and ground-based telescopes. The SOIR instrument onboard Venus Express measured its abundance as less than ~50 ppb at the cloud top (~70 km) increasing to 1 ppm in the upper atmosphere (~110 km). Such a vertical trend conflicts with the vertically constant profile (up to ~80 km) reported by sub-mm ground-based observations. Near-infrared ground-based observations also showed the HCl abundance at the cloud top as ~500 ppb, which are nearly one order of magnitude larger than the SOIR results. The reason for this inconsistency has not been understood yet.
In order to re-examine HCl abundance at the cloud top, we carried out a high-resolution spectroscopy of Venus' dayside at wavelengths of 3.18-3.46 μm and 3.58-4.16 μm with IRTF/iSHELL on August 5-7, 2018 (UT). Taking the full advantages of its high spectral resolution of R ~ 75,000, iSHELL resolved individual HCl lines with sufficient separation from terrestrial lines. In this presentation, we will show initial results of HCl abundance at the cloud top, retrieved from processed spectra and compare them with previous studies. A preliminary report of additional iSHELL observations planned on August 18-20, 2020 (UT) will also be included.

R009-18
Zoom meeting D ：11/1　PM2　(15:45-17:30)
15:45-16:00

金星大気のスーパーローテーションに流される紫外波長の雲形態の時間発展

#須田　智也[1)],今村　剛[2)]
[1)]東京大学,[2)]東京大学

Temporal evolution of cloud morphology at ultraviolet wavelengths advected by super rotation

#Tomoya Suda[1)], Takeshi Imamura[2)]
[1)]The University of Tokyo,[2)]The University of Tokyo

In order to understand the mechanism by which Venus's cloud is maintained dynamically and chemically, it is necessary to clarify the transport of atmospheric constituents on various temporal and spatial scales. In the ultraviolet images of Venus, various small-scale patterns such as convection and streaks are seen on the cloud top. Though their relation to material transport has been drawing attention, their dynamical properties and contribution to transport are not known. These patterns are advected by the high-speed easterly wind called the superrotation, and the investigation of their evolution over time would provide clues to the process. Therefore, we performed such an analysis using ultraviolet images taken continuously at the wavelength of 283 nm by the Venus probe Akatsuki. SO_2 is the dominant absorber at 283 nm on Venus, and the horizontal distributions of SO_2 and clouds near the altitude of 65 km can be observed. By projecting these images onto a coordinate system that moves westward at the speed of the superrotation, we can track individual air parcels while they appear on the morning side of Venus, pass through the noon region, and then disappear on the evening side. In this way, it is possible to observe how each convective pattern changes along the local time. We further evaluate the pattern changes quantitatively and examines the statistical tendency of the pattern change depending on local time. Such information is expected to lead to the elucidation of the temporal and spatial scales of small-scale processes such as convection and the factors that control them.

金星の雲が力学的，化学的に維持される仕組みを理解するために，様々な時間・空間スケールの物質輸送を明らかにする必要がある．金星の紫外画像には雲頂に対流状や筋状など様々な小スケールの模様が見られ，物質輸送との関わりが注目されているが，力学的性質も輸送への具体的な寄与もわかっていない．これらの模様はスーパーローテーションと呼ばれている高速の東風に流されており，その過程でどのように時間発展するのかを調べることで手がかりが得られることが期待されるが，未だそのような研究はなされていない．そこで我々は，金星探査機あかつきによって連続的に撮影された波長 283nm の紫外画像を用いてそのような解析を行った．金星での 283nm の紫外吸収物質は SO_2 が支配的であり，高度 65km 付近の SO_2 と雲の水平分布を観察することができる．これらの画像をスーパーローテーションの速さで西向きに動く座標系に投影し，個々の空気塊が金星の朝側に現れ，正午の領域を通過したのち夕方側に消え去るまでを追跡する．こうして，ローカルタイムに沿って個々の対流状の模様が変化していく様子を確認することができた．この研究ではさらに，模様の変化を定量的に評価し，模様がローカルタイムに依存してどうのように変化していくのかという統計的傾向を調べる．このような情報は，金星大気の対流など小規模なプロセスの時間・空間スケールとそれらを支配する要因の解明につながることが期待できる．

R009-19
Zoom meeting D ：11/1　PM2　(15:45-17:30)
16:00-16:15

低温度星周りの系外惑星の高層大気における酸素原子のエネルギー状態について

#村岡　徹[1)],亀田　真吾[1)],藤原　均[2)]
[1)]立教大,[2)]成蹊大・理工

The numerical simulation of the energy state of atomic oxygen at the exosphere of exoplanets around the low mass stars

#Toru Muraoka[1)], Shingo Kameda[1)], Hitoshi Fujiwara[2)]
[1)]Rikkyo Univ.,[2)]Faculty of Science and Technology, Seikei University

The exoplanet is a planet that orbits a star other than the sun. To date, more than 4000 exoplanets have been detected. Transit photometry is one of the methods to detect the exoplanets by observing the drop of the host star's brightness when the planet transits in front of the host star.
Many exoplanets have been detected by this method.
In recent years, systems with planets considered to be terrestrial planets located in the habitable zone (HZ), such as the TRAPPIST-1 system, have been discovered. However, it is difficult to determine whether these planets' life activities can be expected or not only by detecting the planets.
Transit spectroscopy, which can observe an exoplanetary atmosphere, is a means of solving this problem.
We can estimate the exoplanet's surface environment when we detect the deeper drop of brightness by transit spectroscopy than the drop by Transit photometry.
In this study, we focus on atomic oxygen with emission line wavelengths of ~130 nm from the perspective of biomarkers and ease of observation.
K-type and M-type stars, which are smaller than the sun, are relatively active. So exoplanets, located in their HZ, receive intense XUV radiation (10-100 nm). If the planet had an atmosphere rich in oxygen and poor in carbon dioxide (Earth-like), the atmosphere is thought to be heated by ionization/dissociation heat and expand to a very high altitude. This consideration will work in favor of detecting the atomic Oxygen by Transit photometry.
The World Space Observatory-UV (WSO-UV) is a multi-national space telescope project, led by Russia, to be launched in 2025. The critical scientific objective would involve studying extrasolar planetary atmospheres in the presence of intense UV radiation fields.
The goal of this study is to find exoplanets with the same environment as Earth. First, we calculated the spread of oxygen atoms when there was the Earth in each HZ of M-type star TRAPPIST-1 and K-type star HD85512. Subsequently, we simulated transit spectroscopy observation by WSO-UV and calculated the atomic oxygen detection efficiency. Through these works, we considered the possibility of detecting Earth-like exoplanets.
Last year, we only considered spontaneous emission to calculate the transition of the energy levels and distribution of atomic oxygen at the exosphere.
This time, we newly applied the excitation of atomic oxygen by considering absorption of the oxygen emission line from the host star to calculate the transition of the energy levels. Then, we assumed the light curves to calculate the number of observations necessary for detection. We are planning to announce the results of our calculation of atomic oxygen detectability.

系外惑星とは、太陽以外の恒星の周りを回る惑星である。現在までに 4000 を超える系外惑星が検出されており、その多くは惑星が中心星を横切る（トランジットする）際の減光（中心星からの光の一時的な減衰）を観測する、トランジット観測によって間接的に検出されている。
近年では TRAPPIST-1 系などハビタブルゾーン（HZ）に地球型と思われる惑星を持つ系も発見されてきている。しかしながら、それらの惑星が地球のような、生命活動が期待できる惑星なのか、そうではなく金星や火星のような惑星なのかを決定するには未だ分かっていないことが多い。
そこで、トランジット分光観測という、大気に含まれる元素をあらかじめ推定し、分光観測によってその輝線の波長でトランジット観測を行う方法による、系外惑星の表層環境推定という試みがなされている。本研究ではバイオマーカーという観点や観測のしやすさなどから、輝線波長~130nm の酸素原子に注目している。
観測ターゲットとしては、太陽より小さい、スペクトル K 型や M 型の星が挙げられる。これらの星は比較的活動が活発なため、その HZ に位置する系外惑星は強力な XUV 放射（10-100 nm 程度の紫外線）を受ける。このとき惑星が、二酸化炭素が少なく酸素が豊富な大気を持っていた場合、大気は電離熱・解離熱などで加熱され、非常に高高度まで膨張すると考えられており、このことはトランジット分光観測に有利に働くと考えられる。
一方、World Space Observatory-UV(WSO-UV)は現在ロシアが計画中の紫外線宇宙望遠鏡であり、2025 年に打ち上げ予定である。WSO-UV 計画の主な科学目的として、高 UV 環境下での系外惑星大気の研究が挙げられている。
本研究の大目標は地球と同じような環境の系外惑星を見つけることである。そのために、まず M 型星の TRAPPIST-1、そして K 型星の HD85512 の各 HZ に地球があった場合の酸素原子の広がりを計算した。続いて、そのときの酸

素原子検出効率を、WSO-UV によるトランジット分光観測を模擬して計算し、各恒星周辺における系外惑星大気の酸素原子検出可能性を考察した。
昨年は地球大気の観測結果と整合性の取れている 1 次元モデル[Fujiwara doctor's thesis (1996)]を用いた外圏底以下の中間圏~熱圏のシミュレーションに加え、外圏での自然放射による酸素原子のエネルギー準位の変化を考慮した酸素原子分布を計算し、WSO-UV による観測シミュレーションに応用した。今回は酸素原子分布の計算に、新たに恒星からの酸素輝線を吸収することによる励起を考慮した計算や、ライトカーブから検出に必要な観測回数を求めた計算を加え、系外惑星の酸素原子検出可能性について検討した結果を発表する予定である。

R009-20
Zoom meeting D ：11/1　PM2　(15:45-17:30)
16:15-16:30

南極昭和基地での木星極域ヘイズの偏光観測

#二村　有希[1)],高橋　幸弘[1)],高木　聖子[1)],佐藤　光輝[1)]
[1)]北大

Polarimetric observation of Jupiter polar haze at Syowa Station, Antarctica

#Yuki FUTAMURA[1)]
[1)]Hokkaido University

The stratosphere in the polar region of Jupiter has denser haze than other latitudinal regions. It is known that the polar haze has a cap-like feature, and its edge shows a wavy structure. However, there are a limited number of long-term observations, and their dynamics have not been investigated in detail. Polarization observation is effective for investigating physical parameters such as haze particle size and optical thickness, but there are only a few examples of observation for the structure in the longitudinal direction.
In this study, we conducted polarization imaging of Jupiter at Syowa Station in Antarctica, where you can see Jupiter at high altitude (10 degrees or more in elevation) for a period exceeding Jupiter's rotation cycle (about 10 hours), every 5 months during the winter season in Antarctica in 2019. As a result, valid data were obtained for a total of 13 days, and the longest continuous observation per observation was 14 hours. Polar haze was observed in the wavelength range of 890±5 nm using a bandpass filter including the methane absorption wavelength range.
As an initial analysis, the Jupiter image was magnified and adjusted in position, the peripheral extinction was corrected, the haze region was determined from the latitude distribution of brightness, and the polarization degree of that region was obtained. We will report the variation of the degree of polarization as a function of longitude and its variation on the time scale of days and months.

木星極域の成層圏には、低・中緯度に比べてヘイズが多く存在する。メタン吸収波長で観測すると、極域ヘイズは冠状の構造をしており、その外周に沿って波状構造が見られるという特徴が知られている。しかし、長期的に継続した観測は少なく、その動態は詳しく調べられていない。また、ヘイズの粒径や光学的厚さといった物理パラメーターを調べるには偏光観測が有効であるが、それによる経度方向の構造を調べた例はほとんどない。
本研究では、木星の自転周期(約 10 時間)を超える時間、高高度(仰角 10° 以上)で木星を見ることが可能な南極昭和基地で、2019 年南極越冬期間中毎月一晩以上の撮像偏光観測を 5 ヶ月間実施した。その結果、のべ 13 日間有効なデータが得られ、1 回あたりの最長の連続観測は 14 時間であった。メタン吸収波長帯を含む 890±5 nm のバンドパスフィルターを用いて木星を観測したので、極域ヘイズは明るく見える。初期解析として、木星画像を拡大し位置調整した後、周辺減光を補正し、明るさの緯度分布からヘイズ域を決定し、その領域の偏光度を求めた。木星の経度の違いによる偏光度の変動及び、数日・数ヶ月の時間スケールでのその変動について報告する。

R009-21
Zoom meeting D ：11/1　PM2　(15:45-17:30)
16:30-16:45

2018 年から 2020 年の海王星ストームの移動速度と規模の推定

#佐藤　佑樹[1)],高橋　幸弘[1)],佐藤　光輝[1)],高木　聖子[1)],今井　正尭[2)],大野　辰遼[1)]
[1)]北大・理・宇宙,[2)]産総研

Estimation of the drift rate and intensity of Neptune's storm in 2018-2020

#Sato Yuki[1)], Yukihiro Takahashi[1)], Mitsuteru SATO[1)], Seiko Takagi[1)], Masataka Imai[2)], Tatsuharu Ohno[1)]
[1)]Cosmosciences, Hokkaido Univ.,[2)]AIST

A storm more than 4,000 km in diameter occasionally occurs in Neptune. In a previous study, Voyager 2 observed Neptune on May 24, 1989, and discovered a storm of 13,000 km in diameter called Great Dark Spot(GDS). GDS was located in the southern hemisphere like the Great Red Spot of Jupiter. But GDS became extinct when the Hubble Space Telescope observed it in 1994 (Hammel et al., 1995). It is unknown whether it is a sudden thing or storms such as GDS always occur in Neptune. In addition, a huge storm of 9,000 km was observed on July 2 and June 26, 2017, by Keck observatory (Edward et al., 2019). It's considered that Neptune storms occur at a mid-latitude in the north and south that an ascending air occurs. However, this huge storm occurred near the equator. Neptune's rotation axis is 29.6 deg, and the storm possibly occurred near the equator because of seasonal change. Neptune is observed by large telescopes such as Keck observatory and the Hubble Space Telescope, but it isn't easy to always use those telescopes for Neptune observation. Therefore Neptune is not observed for the long term on a short time scale. We developed the technique to estimate the drift rate and intensity of storms by observing Neptune's whole spectrum in this study. When seeing is bad, it's possible to observe and acquire Neptune's observation data for the long term on a short time scale. The purpose is to deepen the understanding of Neptune's atmosphere convection structure by chasing the detailed change of storms. In this study, we observed Neptune by using 1.6 m Pirka telescope that Hokkaido University owns. The observation time is from October 22, 2018, to November 26, 2018, from July 8 to November 12, 2019, and we started observation on July 20 in 2020. The wavelengths are 890, 855 nm. In this study, we used a methane absorption of 890 nm. Storms look brighter at 890 nm because the altitude of storms is higher than that of other areas. In addition, the apparent size of storms from the observation point changes by the rotation of Neptune, so an 890 nm flux changes by the rotation. We took the ratio of an 890 nm flux and an 855 nm flux to correct the atmosphere's effect of the earth and calculated the theoretical values of the relative intensity by the rotation. We assumed storm's area and fit the observed values with the theoretical values in the method of least squares to estimate the drift rate and 890 nm reflectance inside storms. We estimated that the drift rate and the 890 nm reflectance are 24.6 deg/ day and 0.055 in 2018, respectively. In 2019, we assumed that there are a few storms and estimated that the drift rate and 890 nm reflectance of the first storm is 22.8 deg/day and 0.128, those of the second one is 39.6 deg/day and 0.081, those of the third one is 51.9 deg/day and 0.149, respectively. In 2018, Simon et al. (2019) discovered a new northern Great Dark Spot (NDS-2018) located at 23 degrees N. NDS2018 drifted westward at 2.46 deg/hr in November 2018. However, NDS-2018 could not be seen because it was located on the night side during our observation, and it is considered that we observed a different storm. We will continue observation in 2020, compare with other researchers and amateur observations, and have a discussion in the future.

海王星では直径が 4,000 km を超える巨大なストームが時折発生している。先行研究では ，ボイジャー2 号が 1989 年 5 月 24 日に海王星を観測し，大暗斑と呼ばれる直径 13,000 km のストームを発見した．大暗斑は木星の大赤斑と同様南半球に位置していたが，その後，ハッブル宇宙望遠鏡が 1994 年に観測したところ，大暗斑は消滅していた (Hammel et al., 1995)．大暗斑のようなストームは海王星で常に発生しているのか，突発的なものなのか不明である．また，直径 9,000 km のストームが 2017 年 6 月 26 日, 7 月 2 日にケック天文台 10 m 光学近赤外望遠鏡で観測された (Edward et al., 2019)．通常，海王星のストームは上昇気流が発生している南北の中緯度で発生すると考えられている．しかし，このストームは赤道付近で発生している．海王星の自転軸傾斜角は 29.6 度であり，季節変化によって赤道付近でストームが発生した可能性も考えられる．ケック天文台やハッブル宇宙望遠鏡によって海王星は観測されているが，それらの望遠鏡を常に海王星観測に使用することは難しい．そのため，短い時間スケールで長期的な海王星ストームの観測は行われていない．本研究では海王星全体のスペクトルを観測することによって，ストームの移動速度や規模を推定する手法の開発を行った．それにより，シーイングが悪い時でも観測可能になり，短い時間間隔で長期的な海王星ストームの観測データを取得することができるようになった．この手法で，ストームの詳細な変動を追うことで，海王星大気の対流構造の理解を深めることに繋げる．本研究では，北海道大学が所有する口径 1.6 m のピリカ望遠鏡を用いて海王星のスペクトルを観測した．時期 は 2018 年 10 月 22 日から 11 月 26 日, 2019 年 7 月 8 日から 11 月 12 日, 2020 年は 7 月 20 日から観測を開始した．観測波長は 890, 855 nm である．本研究では，メタンが 890 nm を強く吸収するという性質を用いる．海王星大気にはメタンが存在し, 890 nm で海王星を観測すると，周りの領域よりも高度の高いストームはより明るく見える．よって，ストームがある面を観測すると 890 nm フラックスは大きくなる．また，海王星の自転によって，観測点からのストームの見た目の大きさは変化するため, 890 nm のフラックスも変化する．地球大気の影響を補正するために, 890 nm フラックスと 855nm のフラックスの比をとり，相対強度を求めた．890 nm フラックスの相対強度の理論値を求め，その理論値と観測値を最小二乗法でフィッティ

ングをすることで，ストームの移動速度や規模を見積もった．ストームの面積を仮定しストーム内部の 890 nm 反射率を求め，ストームの規模は面積と反射率の積とした. 2018 年のストームの移動速度, 890nm アルベドは 24.6° / day, 0.055, 2019 年は複数のストームがあると仮定し，1 つ目は 22.8°/day, 0.128, 2 つ目は 39.6° / day, 0.081, 3 つ目は 51.9° / day, 0.149 と推定した. 2018 年に, Simon et al. (2019)によって北緯 23° に位置し, 2.46°/hr (59.04°/day) で移動するストーム（NDS-2018)が観測された．しかし，NDS-2018 は我々の観測日では裏面に位置し見ることはできず、違うストームを観測したと考えられる。2020 年も観測を継続し、他の研究者やアマチュア観測と比較し、今後議論を進める。

R009-22
Zoom meeting D ：11/2 AM1 (9:00-10:30)
09:00-09:15

Retrieval of vertical structure in the Martian atmosphere during 2007 global dust storm by OMEGA/MEx limb observation

#Risei Kogure[1)], Arnaud Mahieux[2),4)], Hiromu Nakagawa[3)], Shohei Aoki[2),5)], Yasumasa Kasaba[1)], Nao Yoshida[3)]
[1)]Tohoku Univ.,[2)]BIRA-IASB,[3)]Geophysics, Tohoku Univ.,[4)]University of Texas at Austin, USA,[5)]LPAP , Belgium and FNRS, Belgium

Recent observations have revealed an unexpected high abundance of water vapor in the middle atmosphere, which may be able to drive the enhancement of the atomic hydrogen escape (Chaffin et al., 2017; Fedorova et al., 2018, 2020; Heavens et al., 2018; Vandaele et al., 2019; Aoki et al., 2019). However, it is unclear how to extract water vapor from the lower atmosphere and place it in the middle atmosphere, since the vertical propagation of water vapor is limited by 'the cold trap' at its condensation level. The cold trap confines water in the lower atmosphere by its freezing out. Effective water vapor transportation into the middle atmosphere has been proposed by an inflation of the lower atmosphere, due to the sunlight absorbed by the upsurge of dust associated with intensified meridional circulation can (Aoki et al., 2019; Neary et al., 2019). For the comprehensive picture of the water transport and the background atmospheric condition in the middle atmosphere, two-dimensional (vertical vs latitudinal) distribution of physical parameters is needed to clarify the transient phenomena, such as a rocket dust storm (Spiga et al., 2013).
In this study, we aim to present the 2D vertical structures of water vapor, dust opacity, and CO2 non-local thermal equilibrium (LTE) emission in the periods of 2007 global dust storm (Ls = 265-305) using the OMEGA limb observation onboard Mars Express. The indexes of water vapor and dust opacity are obtained from the wavelength ratio between 2.50 and 2.64 μm and the radiance at 2.77 μm, respectively. CO2 non-LTE emission is seen at 4.3 μm. From the slope of the observed spectrum between 0.5 and 3.0 μm, the effective radius of aerosol particles is estimated. As the reference, observations during the global dust storm in Orbit-4483 (Ls = 268) and Orbit-4621 (Ls = 292) is compared with that at clear-sky season in Orbit-291 (Ls = 17) and Orbit-647 (Ls = 64). The preliminary results are summarized as follows.
(1) The observed radiance at 2.77μm increase up to 50~55km altitude at Orbit-4483 during the global dust storm compared to clear-sky at Orbit-291. This could be caused by suspended dust.
(2) The slopes of observed spectra suggest a larger particle size at 40 km during the global dust storm at Orbit-4483 (~1.0 μm) than that in the clear-sky at Orbit-291 (~0.4 μm). This is comparable with previous studies.
(3) We confirmed that the CO2 non-LTE emission peaks at higher altitudes (100-120 km) during the global dust storm in Orbit-4483. This result basically suggests about 20 km increase of peak altitudes comparing with that in the clear-sky at Orbit-291. This can be explained by the heating by absorption of incoming sunlight via suspended dust particles.
(4) The water vapor exists up to 55 km altitudes at Orbit-4483 during the global dust storm. This is totally different from that at Orbit-647 at clear-sky season, which shows the confined water vapor up to ~30 km altitude. This water vapor transportation to high altitude may occurred due to the results of (1) ~ (3).

R009-23
Zoom meeting D ：11/2 AM1 (9:00-10:30)
09:15-09:30

Intense zonal wind in the Martian mesosphere during the 2018 planet-encircling dust event observed by IR heterodyne spectroscopy

#Akiho Miyamoto[1)], Hiromu Nakagawa[1)], Takeshi Kuroda[1)], Kosuke Takami[1)], Isao Murata[1)], Nao Yoshida[1)], Katsushige Toriumi[1)], Shohei Aoki[2)], Hideo Sagawa[3)], Yasumasa Kasaba[1)], Naoki Terada[1)]
[1)]Science, Tohoku Univ.,[2)]BIRA-IASB,[3)]Kyoto Sangyo University

In the Martian atmosphere, the suspended dust absorbs incoming sunlight and contributes to localized atmospheric heating. On June 2018, a planet-encircling dust event (PEDE) occurred on Mars. The growth phase of the dust event is Ls=195-220 and the decay phase is Ls=220-260 [Aoki et al., 2019]. The water vapor has been transported up to 100 km during the dust event in both north and south hemispheres [Fedorova et al., 2020]. The model predicted that the distribution of water vapor is associated with that of Hadley circulation reinforced by the dust event [Neary et al., 2019]. Mesospheric circulation on Mars is largely influenced by PEDEs. However the measurement of mesospheric wind is very few. Moreno et al. (2009) observed zonal wind around 50 km during 2001 PEDE by IRAM, which implied prograde acceleration by the dust event. On the other hand, the region around 80 km altitude remains the least explored region with a highly variable nature that deserves extensive measurements during the dust event.

In order to understand the mesospheric dynamics during PEDEs, we have performed the direct measurement of zonal winds around 80 km from June to September 2018 by ground-based infrared heterodyne spectroscopy. The beam size is 4 arcsec for Martian angular diameter about 20 arcsec. The observed CO2 non-local thermodynamic-equilibrium (non-LTE) emission lines at 10 micron are contributed from the mesosphere, peaking at ~ 80 km altitude [Lopez et al., 2011]. The zonal wind velocity was directly derived from line-of-sight (LOS) Doppler shift of emission cores between equational limb of dayside and disk center.

The observed LOS Doppler wind implies retrograde zonal wind in the mesosphere, which agrees with the results observed by previous studies during clear sky [Sonnabend et al., 2012]. By contrast, we detected the large doppler shifts to be 222 m/s on average with the standard variation of about 101 m/s. The observed wind velocities are much larger than those in clear sky (~140 m/s) [Sonnabend et al., 2012].

The uncertainty of retrieved value was roughly estimated to be 46% due to the fitting error, pointing error, and wavelength calibration uncertainty. Even with the large uncertainty, our result suggests an intense retrograde wind in the mesosphere during 2018 PEDE.

Our result was compared with the prediction by the general circulation models (GCMs) [Medvedev et al., 2013; Kuroda et al., 2019]. The models consider zonally averaged latitude-time dust distributions during 2001 and 2018 PEDE observed by MGS, respectively. The models predicted an intense retrograde wind (~80-180 m/s) during the dust event around 0.1 Pa (around 80 km). Our result supports their prediction.

In order to clarify the mechanism to accelerate the zonal wind, we use the horizontal momentum equation in the transformed Eulerian mean (TEM) formalism [Andrews et al., 1987]. By applying the visual confirmation results of Medvedev et al. (2013) and the results of Kuroda et al. (2019) for the formula, it was found that the effects of meridional advection, vertical advection and gravity waves (horizontal total wavenumber of larger than 60) are about 45 m/s・sol, 4 m/s・sol and about 30 m/s・sol at the corresponding region, respectively. The total effect on retrograde wind acceleration is about 80 m/s・sol.

Consequently, it is possible to get the observed retrograde wind velocity (~140 m/s acceleration) for 2~3 sols after the occurrence of 2018 PEDE theoretically mainly due to the gravity waves and the enhanced Hadley cell across the equator during 2018 PEDE. Further observations are needed to confirm our implication.

R009-24
Zoom meeting D ：11/2　AM1　(9:00-10:30)
09:30-09:45

#晝場　清乃[1)],中川　広務[1)],中村　勇貴[1)],堺　正太朗[1)],村田　功[1)2)],寺田　直樹[1)]
[1)]東北大・理・地球物理,[2)]東北大院・環境

MAVEN/IUVS observation of the Martian ozone layer during solar energetic particle events

#Sayano Hiruba[1)], Hiromu Nakagawa[1)], Yuki Nakamura[1)], Shotaro Sakai[1)], Isao Murata[1),2)], Naoki Terada[1)]
[1)]Geophysics, Tohoku Univ.,[2)]Environmental Studies, Tohoku Univ.

Solar Energetic Particles (SEP) consist of protons, electrons and heavy ions in the energy range between a few tens of keV and GeV, which are originated from solar flares in the low corona, shock waves driven by coronal mass ejections (CME), planetary magnetospheres, and bow shock. SEPs are well known to damage not only spacecraft and detectors but also human body. For future international space explorations in the 2020s, the human activity is going to expand to the Moon and Mars. Thus, the impact of SEP on future explorations on Mars needs to be addressed. However, the effect of SEP on the Martian atmosphere and surface environment is not well understood. In addition, SEP penetrates into Earth's atmosphere down to tens of kilometers at high geomagnetic latitudes, which affects the composition in the middle atmosphere. During the large solar flare in October 2003, SEP caused NO_2 enhancement of several hundred percent and tens of percent ozone depletion between 36 and 60 km altitudes (e.g., Seppala et al., 2004; Rohen et al., 2005). In contrast, the vertical distribution of ozone on Mars was extensively observed by SPICAM onboard Mars Express from 2004 to 2014. Results of previous studies show that the ozone layer was located around 50 km altitude in the southern polar winter, and around 30-40 km altitude in low to middle latitudes in both hemispheres at aphelion season (Montmessin et al., 2013, Maattanen et al., 2019).
Mars has a thin atmosphere, less than 1% of that on Earth. The surface and atmosphere are heavily affected by energetic photons and particles that easily penetrate it owing to insufficient magnetospheric and atmospheric shielding. The Imaging UltraViolet Spectrograph (IUVS) spectroscopy onboard Mars Atmosphere and Volatile EvolutioN(MAVEN) detected diffuse aurora, suggesting widespread occurrences with increased SEPs (Schneider et al., 2015; Schneider et al., 2018). Schneider et al. (2018) reported the low-altitude, "diffuse" aurora spanning across Mars' nightside hemisphere, coincident with a SEP outburst. The emission extended down to an altitude of ~60 km. Deep precipitation in the middle atmosphere requires extremely energetic electron fluxes up to 100 keV. This fact suggests that SEP may have additional effects on global atmospheric structures in the Martian atmosphere. Incident particles ionize and dissociate atmospheric species deeply, as well as heat the target atmosphere.
The purpose of this study is to investigate the effects of SEP on the Martian atmosphere, especially on ozone, which will help us to understand the study of astrobiology and the greenhouse effect of the early Martian atmosphere.
In this study, we use vertical profiles of ozone, carbon dioxide, and oxygen number densities observed by stellar occultation measurements by Imaging UltraViolet Spectrograph (IUVS) on board Mars Atmosphere and Volatile EvolutioN (MAVEN), and the energy fluxes of electrons and ions by Solar Energetic Particles onboard MAVEN (MAVEN/SEP). Since March 2015, MAVEN/IUVS has generally conducted stellar occultation campaign for 1-2 days on average for every 2-3 months. MAVEN/IUVS observations cover whole longitudinal area, and wide range of latitudes from 80° S to 75° N. MAVEN/SEP detects an energy spectrum of electrons from 30 keV to 1 MeV and ions from 30 keV to 12 MeV up to 10-10^6 eV/[cm^2 s sr eV].
The distribution of ozone observed by MAVEN/IUVS confirms the seasonal, latitudinal and altitudinal characteristics of the ozone distribution observed by MEX/SPICAM. MAVEN/IUVS observations show the peak number density of ozone to be the order of 10^8 /cc at the southern polar winter and the order of 10^9/cc for both hemispheres at aphelion season. These peak number densities are generally well in agreement with the SPICAM observation, but some data are not quantitatively consistent in detail.
Using the MAVEN/SEP, we analyzed the energy fluxes of solar energetic particles observed between March 2014 and January 2020 in order to identify the periods of strong solar energetic particle arrival events, related to the IUVS observations. Here, we focus on two events; One occurred in 25-26th March 2015 for 39 hours before and after the arrival of electrons of SEP, with 20 occultation profiles, and the other occurred in 3-4th November 2015 for 27 hours after the arrival of electrons to the arrival of ions, with 34 profiles. The effect of SEP on the atmosphere is addressed by comparing with 26 profiles in 8-9 October 2017 during the quiet period.

太陽高エネルギー粒子(Solar Energetic Particles：SEP)は陽子や電子、重イオンから構成される数十 keV から数 GeV の粒子である。これらはコロナ質量放出や太陽フレアと呼ばれる爆発現象に伴って惑星間空間に大量に放出され伝搬していくことが知られている。太陽高エネルギー粒子は探査機・検出器などに損傷を起こすことでも知られているだけでなく、人体にも被曝により悪影響を及ぼす。2020 年代の国際宇宙探査到来とともに人類の活動領域が月、そして火星へと急速に広がりつつある中で、火星で有人あるいは無人活動を行う際に、太陽高エネルギー粒子の影響は極めて大きい。しかし、火星周辺における太陽高エネルギー粒子が火星大気・表層環境にどのような影響を与えるのか解明されていないため、その予測は困難である。またその影響は宇宙空間にとどまらず、地球の高磁気緯度領域の高度数十 km にまで侵入し中層大気の大気組成の変化をも引き起こす。2003 年 10 月の大型フレア時には、太陽高エ

ネルギー粒子到来に伴って地球大気中の NO_2 増加と、それに伴うオゾン層の半減が報告されている(e.g., Sepp?l? et al., 2004; Rohen et al., 2005)。
一方、火星におけるオゾン鉛直分布は、2004 年から 2014 年まで Mars Express 搭載の SPICAM が精力的に観測を実施してきた。この先行研究の結果によると、冬の南極では約 50 km にオゾン層が存在することが分かっている。加えて遠日点では、両半球とも低中緯度にて 30〜40 km でオゾン層が観測されている(Montmessin et al., 2013, Maattanen et al., 2019)。
火星は大気圧が地球の約 1/100 かつ固有磁場をもたないため、太陽高エネルギー粒子の影響は地球磁気圏内に比べて甚大である。それは、2017 年 9 月の SEP イベント時に、火星夜側全球が大気化学反応を介してオーロラのように発光する現象が発見されたことからも明らかであり、100 keV 以上の太陽高エネルギー粒子が高度 70 km 程度まで降り込んでくることが示唆された(Schneider et al., 2018)。太陽高エネルギー粒子が火星大気において中性大気の電離や加熱、大気化学反応による組成変化など、全球的に大気構造に大きく影響を与える可能性があると考えられる。本研究の目的は、太陽高エネルギー粒子が火星大気、特にオゾンに与える影響を調べることであり、これによってアストロバイオロジーの観点や過去火星の温室効果について解明することに繋がると考える。本研究で我々は、NASA 火星探査衛星 Mars Atmosphere and Volatile EvolutioN(MAVEN)搭載 Imaging UltraViolet Spectrograph(IUVS)による星掩蔽観測から得られたオゾン、二酸化炭素、酸素の数密度鉛直分布に加え、同衛星搭載 Solar Energetic Particles(SEP)から火星周回軌道上における太陽高エネルギー粒子の電子・イオンのエネルギーフラックスのデータを用いた。IUVS は 2015 年 3 月から、平均で 2〜3 ヶ月ごとに 1 度の頻度で 1〜2 日間の星掩蔽観測キャンペーンを継続的に行ってきた。この星掩蔽観測は南緯 80 度から北緯 75 度までと、経度全範囲を広くカバーしている。SEP は、電子は 30 keV〜1 MeV、イオンは 30 keV 〜12 MeV のエネルギースペクトルを $10〜10^6$ eV/[cm^2 s sr eV]の範囲で観測することができる。
MAVEN/IUVS で観測されたオゾンの分布から、MEX/SPICAM で観測されたオゾン分布の季節・緯度・高度の特徴を確認することできた。また、IUVS の観測では南極の冬でのピーク高度では 10^8 /cc のオーダーの数密度をとり、遠日点においては両半球共に約 10^9 /cc のオーダーをとっている。この数密度に関しては、SPICAM の観測と概ね一致するものの、詳細には量的に一致しないデータも存在する。
2014 年 3 月から 2020 年 1 月までに MAVEN/SEP が観測した太陽高エネルギー粒子のエネルギーフラックスを解析し、大規模な SEP イベントで、IUVS の星掩蔽観測から得られた大気密度データが存在する 2 つのイベントに着目して解析を行った。1 つ目は、2015 年 3 月 25〜26 日の太陽高エネルギー電子の到来前から到来後までの約 39 時間のデータ、2 つ目は、2015 年 11 月 3〜4 日の電子到来後からイオン到来までの約 27 時間のデータである。本発表では、大規模 SEP イベント時のデータ解析を行い、比較的季節・緯度が同じ 2017 年 10 月 8〜9 日の静穏時データとを比較することで、太陽高エネルギー粒子が大気に与える影響を明らかにする。

R009-25
Zoom meeting D ：11/2 AM1 (9:00-10:30)
09:45-10:00

Day-night variation of O2/CO2 in Mars lower thermosphere

#Hiromu Nakagawa[1)], Nao Yoshida[1)], Naoki Terada[1)], Hitoshi Fujiwara[2)], Takeshi Imamura[3)], Kaori Terada[1)], Kanako Seki[4)], Nicholas M. Schneider[5)], Sonal Jain[5)], Roger V. Yelle[6)], Franck Montmessin[7)], Hannes Groller[6)], Bruce M. Jakosky[8)]
[1)]Dept. Geophys., Grad. Sch. Sci., Tohoku Univ.,[2)]Faculty of Science and Technology, Seikei University,[3)]The University of Tokyo,[4)]Dept. Earth & Planetary Sci., Science, Univ. Tokyo,[5)]LASP, Univ. of Colorado,[6)]University of Arizona,[7)]LATMOS,[8)]LASP, CU Boulder

The location of a compositional boundary, the homopause, influences theremospheric composition and thereby the escape of the species to space. We report detection of the homopause, for O_2/CO_2 profiles on Mars made by the Mars Atmosphere and Volalite EvolutioN/Imaging Ultraviolet Spectrograph, which allows us to study the vertical structure of the atmospheric compositions of O_2 and CO_2 in the 20 to 150 km altitude region (Groller et al., 2015, 2018). Our inferred O_2 and CO_2 density profiles have a typical vertical resolution of 2 to 10 km, which is smaller than or equal to the averaged atmospheric scale height (6 to 12 km, depending on altitude). The O_2/CO_2 ratio below the homopause is equal to the values of well-mixed homosphere; while, the O_2/CO_2 ratio above the homopause is enhanced by diffusive separation. The altitudes of the homopause substantially varies with latitude, season, and local-time in the range between 100 and 150 km. The predictions of the Mars Climate Database (Millour et al., 2012), however, systematically underestimate the altitudes of homopause by ~20 km. At a certain pressure level, we find that the variation of homopause is not obvious between day and night in the first half of the Martian Year. This suggests that inflation and contraction of the lower atmosphere can explain the variation of homopause. Meanwhile, the variation of homopause in the latter half of the Martian Year is noticeably difference between day and night. The inferred eddy diffusion coefficients at homopause are in the range between 10^7 and 10^8 cm^2s^{-1}. This reasonably agrees with the extrapolated results by previous studies (Izakov, 1978; Slipski et al., 2018). Time constant of diffusion must be order of 10^4 to 10^5 s (hours to days). The day-night variation can be explained as a signature of the global circulation in the upper atmosphere, in addition to the difference of eddy diffusion coefficient. Our result may imply a strong upwelling on the dayside and subsidence on the nightside. This enhances more fractions of lighter species on the nightside. This process is well known on the Earth, and especially Venus, where the nightside bulges in H and He are factors of hundreds and thousands in the thermosphere. Similar physics can work on Mars, as reported by Elrod et al (2016) which represented the He bulge in Mars thermosphere. The classical diffusion calculations are made to demonstrate the considerations discussed above.

R009-26
Zoom meeting D ：11/2　AM1　(9:00-10:30)
10:00-10:15

中間赤外中空ファイバを用いたレーザーヘテロダイン分光器の信号取得効率の評価

#塚田　悟輝[1)],中川　広務[2)],村田　功[3)],平原　靖大[4)],笠羽　康正[5)],片桐　崇史[6)],松浦　祐司[7)],宮本　明歩[1)],山崎敦[8)]
[1)]東北大・理,[2)]東北大・理・地球物理,[3)]東北大院・環境,[4)]名大・院・環境・地球惑星,[5)]東北大・理,[6)]富山大,[7)]東北大・医工学,[8)]JAXA/宇宙研

Evaluation of the efficiency of the mid-IR laser heterodyne spectrometer using hollow fibers

#Satoki Tsukada[1)], Hiromu Nakagawa[2)], Isao Murata[3)], Yasuhiro Hirahara[4)], Yasumasa Kasaba[5)], Takashi Katagiri[6)], Yuji Matsuura[7)], Akiho Miyamoto[1)], Atsushi Yamazaki[8)]
[1)]Science, Tohoku Univ.,[2)]Geophysics, Tohoku Univ.,[3)]Environmental Studies, Tohoku Univ.,[4)]Earth&Planetary Sciences, Nagoya Univ.,[5)]Tohoku Univ.,[6)]Toyama Univ.,[7)]Biomedical Engineering, Tohoku University,[8)]JAXA/ISAS

The mid-IR laser heterodyne spectroscopy provides high spectral resolution > 10^6, which is much greater than other direct spectroscopic measurements, by combining an IR source from the observing target and an IR laser, such as a quantum cascade laser (QCL) and/or a CO_2 gas laser, as the local oscillator (LO). We have developed the mid-infrared laser heterodyne spectrometer MILAHI (Mid Infrared LAser Heterodyne Instrument) mounted on our dedicated Tohoku 60 cm telescope (T60) at the summit of Mt. Haleakala, Hawaii, which has successfully operated for measurements of Venusian and Martian atmosphere (Nakagawa et al., 2016, Takami et al., 2020).

The two beams are combined at the ZnSe beam splitter and then focused onto a HgCdTe photomixer. A precise optical alignment is required to combine two beams. Since the observable wavelength of a single feedback (FB)-QCL is restricted in the range of several cm^{-1}, switching LOs is needed in order to observe various molecular lines. A CO_2 gas laser covers some parts of the wavelength ranges of 9-12 μm and four QCLs provide the wavelength ranges of 7.43-7.44 μm, 7.71-7.73 μm, 9.54-9.59 μm, 10.28-10.33 μm are installed in MILAHI as LOs. A smooth switching mechanism of LOs is essential for applications of planetary atmosphere. In this study, we aim to simplify the optics, especially to provide a switching mechanism of LOs, by applying mid-IR transmissive hollow fibers.

There is few optical fiber which has a high transmittance at the wavelengths longer than 2 μm. Recently mid-IR (5-20 μm) transmissive hollow fibers has been developed by Tohoku University (e.g. Matsuura et al., 2002). The fibers are made of glass tubing whose inner diameter are 1 mm and have a metallic layer of Ag on the inside of glass tubing and then a dielectric layer of AgI over the metallic layer. Transmittance of 95 %/m at 10.6 μm was reported in previous studies (e.g. George and Harrington, 2004), meanwhile we have achieved about 70% transmittance with a 300 mm hollow fiber at 10.4 μm from our laboratory measurements. Transmittance of hollow fibers strongly depends on its incident angle of the light. Better transmittance might be possible by improving the alignment.

In this study, we evaluate the efficiency of the heterodyne signal using hollow fibers. The following two systems are compared for verifications using a CO_2 gas laser which emits IR at 10.6 μm as a LO and a small blackbody furnace as an IR source.

(i) a conventional system combines two beams using a beam splitter without any fibers
(ii) a fiber system using 300 mm hollow fibers to guide two beams and combines them by a conventional beam splitter

In addition, we have developed the technology related to the fiber coupler and divider (a device enables coupling or splitting lights by combining fibers directly) for the hollow fibers (Tamura et al., 2017) and we will test the efficiency of the heterodyne signal using the fiber coupler. The fiber coupler can provide downsizing, weight saving, high stabilization of the instrument, which are essential to develop the instrument for space-born missions.

レーザーヘテロダイン分光とは、赤外線レーザーの光を局部発信周波数源（Local Oscillator, LO）として、観測対象である惑星からの光を局発光に重ねることで得られる混合光を GH z 帯まで応答する高速赤外線検出器で受信し、超高波長分解能($R = \lambda / d\lambda > 10^6$)を得る分光法で、直接分光法に比べ圧倒的な分解能を誇る。我々はこれまでに、マウイ島ハレアカラ山頂に設置した東北大学望遠鏡 T60（Tohoku 60 cm telescope）に、独自開発した中間赤外レーザーヘテロダイン分光器 MILAHI (Mid Infrared LAser Heterodyne Instrument）を搭載し、金星・火星の大気の観測を実施してきた（Nakagawa et al., 2016; Takami et al., 2020）。現行機では、2 つの光を多数の光学素子で折り曲げて導き、ビームスプリッタで混合しており、各光路で高い位置精度が求められるため光学アライメント調整、特に観測波長域の切り替えには課題を抱えている。それは、MILAHI の観測波長域は LO の発振波長域に依存しており、観測波長域の切り替えには、LO の切り替えが必須であるためである。現在は LO として、7.43-7.44 μm (1343-1346 cm^{-1}), 7.71-7.73 μm (1293-1297cm^{-1}), 9.54-9.59 μm (1043-1048 cm^{-1}), 10.28-10.33 μm (968-973 cm^{-1}）の 4 つの量子カスケードレーザならびに炭酸ガスレーザを所有し、これらを切り替えることで惑星大気中の各成分を観測することが可能となる。本研究では、2 つの光を中間赤外域で高効率の中空ファイバで伝送し、光学系を簡略化、特に LO の切り替えを簡略化することを企図する。

これまで、中間赤外域（5-20 μm）では伝送効率の高い光ファイバが存在しなかったが、近年低損失の中空ファイバ技術が開発され、医工学分野で応用に向けた研究が進められている。本研究では、東北大学医工学研究科で開発が進められてきた、内径 1mm のガラスパイプの内面に銀を蒸着しヨウ化銀でコートした中間赤外中空ファイバを用い

ている(e.g. Matsuura et al., 2002)。先行研究で示されている伝送効率は、波長 10.6 μm の光に対して 95 %/m (e.g. George and Harrington, 2004) である。我々のこれまでの室内実験では、長さ 300 mm の中空ファイバで波長 10.4 μm の光に対して 70 % 程の伝送効率を達成できている。伝送効率は光の入射条件に左右されるため、光の入射方法の改善で、伝送効率の更なる改善が期待される。

本発表では中空ファイバを用いたヘテロダイン分光器の信号取得効率の試験結果を報告する。試験では波長 10.6 μm の赤外線を出射する炭酸ガスレーザーを LO、小型黒体炉を信号光源とする次の 2 つの系の信号強度を比較することで、中空ファイバを用いたレーザーヘテロダイン分光器の信号取得効率を評価する。

① 空気中を伝播した光をビームスプリッタで混合する系

② 信号光・局発光をそれぞれ独立した長さ 300 mm の中空ファイバで伝送し、ビームスプリッタで混合する系

さらに、光ファイバを直接結合することで複数の光の光路を結合・分割できるカップラー技術も発展がめざましく、我々も中空ファイバを用いた光混合・分波器の開発も進めており(Tamura et al., 2017)、今後この光混合・分波器を用いてヘテロダイン信号を取得できるか試験を行う予定である。この光混合・分波器を用いてヘテロダイン信号が得られればファイバに光を入射するだけでヘテロダイン信号が得られるようになるため、従来のヘテロダイン分光器と比較して大幅に光学アライメント調整を簡略化でき、装置の小型化・軽量化、高安定化が実現されることが期待され、将来の飛翔体搭載機器への援用に本質的である。

R009-27
Zoom meeting D ：11/2　AM2　(10:45-12:30)
10:45-11:00

火星のクリュセおよびアキダリア平原における地下構造の探索

#大浦　愛菜[1)],笠羽　康正[1)],野口　里奈[2)],熊本　篤志[1)],石山　謙[3)],臼井　寛裕[2)],土屋　史紀[1)],植村　千尋[4)],木村　智樹[1)]
[1)]東北大学・理・地球物理,[2)]宇宙科学研究所/宇宙航空研究開発機構,[3)]鶴岡工業高等専門学校,[4)]総合研究大学院大学

Search of shallow subsurface reflectors in Chryse and Acidalia Planitiae

#Aina Oura[1)], Yasumasa Kasaba[1)], Rina Noguchi[2)], Atsushi Kumamoto[1)], Ken Ishiyama[3)], Tomohiro Usui[2)], Fuminori Tsuchiya[1)], Chihiro Uemura[4)], Tomoki Kimura[1)]
[1)]Department of Geophysics, Tohoku University,[2)]ISAS/JAXA,[3)]National Institute of Technology Tsuruoka College,[4)]SOKENDAI

Recent studies have investigated the subsurface ice at mid-latitude on Mars (e.g., discoveries of exposed ice sheets [Dundas et al., 2018] and widespread excess ice [Bramson et al., 2015]). In the mid latitude, however, current water ice is unstable as implied by climate models [Schorghofer and Aharonson, 2005]. The discoveries of Martian ice are attributed to high resolution imaging data, spectrometer and/or radar technique. Chryse and Acidalia Planitiae (CAP) are the northern planitiae where subsurface ice layers have not been detected by radar sounding yet.
In this study, we surveyed the region in Chryse/Acidalia Planitiae by the data of Mars SHAllow RADar sounder (SHARAD) provided on Geosciences node of the Planetary Data System (PDS). As Noguchi et al. [2020], we also searched the exposed crater walls close to the candidate reflectors using the data of High Resolution Imaging Science Experiment (HiRISE) images [McEwen et al., 2007]. We estimated the plausible component materials of uppermost layers by using these data.
In this region, we identified several subsurface reflectors, but there was no wide subsurface structure. At two locations, we estimated their dielectric constants of the uppermost layers as 5.3 and 5.9 by the combination with high-resolution images and topographic data. Those values constrained the possible bulk porosity (~25 and ~29 %) and the upper limit for the volume fraction of water ice (~50 %). The estimated porosities suggested that the shallow subsurface layers of those locations could be basalt or till. Volume fraction of water ice for rock-air-ice mixture derived in this study was less than 50 %. Thus, if local ice carried from poles still exists, water ice would be preserved as ice-cemented regolith, not pure water ice.

R009-28
Zoom meeting D ：11/2 AM2 (10:45-12:30)
11:00-11:15

River simulations on early Mars in the Noachian and the Hesperian periods using the global river model, CRIS

Arihiro Kamada[1)], #Takeshi Kuroda[1)], Yasumasa Kasaba[1)], Naoki Terada[1)], Hiromu Nakagawa[1)]
[1)]Geophysics, Tohoku Univ.

The present Mars is cold and arid environment with little stable water on surface. However, the planetary environment on early Mars would have been quite different from that on the current Mars. Many observations have shown geological evidences for the past Martian environment, which should have been warm and wet enough to allow large-scale surface runoff activities. These geological evidences are called as “valley networks (VNs)", which are originated in the boundary between the Late Noachian and Early Hesperian (3.85-3.6 Ga). River might have been an important player for global water and material cycles in the early Mars as well as the present Earth.
We have newly developed a global-scale distributed river model for pan-planets named CRIS (Catchment-based RIver Simulator), which calculates the processes of 1) soil infiltration, 2) river transport, and 3) sediment transport. In the process 1), the storage height and surface, intermediate, and basal runoff in each soil layer are calculated using the model outputs of a paleo-Mars global climate model (PMGCM) [Kamada et al., 2020]. In the process 2), the river discharge and channel parameters are calculated from the runoff volume inputted from 1), assuming the flow down along given channel networks to the ocean and inland lakes. In the process 3), the sediment production and discharges of suspended and traction load are calculated using the river discharge and the channel parameters inputted from 2). The PMGCM assumed a CO2/H2O/H2 atmosphere under the ‘Faint Young Sun' condition (with a solar luminosity of ~75% of the current value) and the pre-True Polar Wander topography [Bouley et al., 2016] assuming the surface condition before late Tharsis formation, for surface pressures of between 0.5 and 2 bar, H2 concentration of between 1 and 6%, obliquity of between 20o and 60o. The horizontal resolution of CRIS is set to 1.125 degrees (~67 km grid interval at the equator), and that of the PMGCM is set to 5.625 degrees (~333 km).
The formation of V-shaped water channels (i.e., VNs) requires a large volume of liquid water combined with stable and long-term fluvial activity, which means that global mean surface temperature above the melting point and enough precipitation should be needed for the early Martian environment. When we assumed an H2-rich (more than 3%) atmosphere, the mean surface temperature rapidly approached and exceeded the melting point as the amount of background CO2 atmosphere increased. Also, the annual precipitation basically increased with surface pressures. Although precipitation on Early Mars is an order of magnitude less than that on Earth, it is enough for intense surface runoff to carve the VNs. Additionally, CRIS predicted that 1) for the obliquity of 20o, significant fluvial and sediment discharges are distributed around Tharsis regions and southern polar regions, although relatively fragile river channels are calculated in VNs regions; 2) for the obliquity of 40o, intense Martian river channels are mainly distributed in equator, seashore, lakeshore regions and Arabia Terra where intense precipitations are observed; and 3) for the obliquity of 60o, there are almost no significant fluvial features in southern low to middle latitudes because annual mean surface temperatures in these regions are less than the melting point of water.
CRIS revealed that warm and wet early Mars with obliquity of 40o would be more plausible to reproduce widespread precipitation-fed river channels across low to middle latitudes. However, even if we consider that Martian VNs are mainly created by rivers, it is not consistent with observations in some areas, such as the Arabia Terra. Recently, Davis et al. [2016] found extensive networks of sinuous ridges in Arabia Terra, which might be interpreted as inverted fluvial channels that formed in the Noachian before being buried. If so, it would be a strong evidence that Martian VNs were made by the ancient river activity.

R009-29
Zoom meeting D ：11/2 AM2 (10:45-12:30)
11:15-11:30

Dependence of ion escape from Mars on ancient solar XUV and solar wind conditions

#Ryoya Sakata[1)], Kanako Seki[1)], Shotaro Sakai[2)], Naoki Terada[2)], Hiroyuki Shinagawa[3)], Takashi Tanaka[4)]
[1)]Dept. Earth & Planetary Sci., Science, Univ. Tokyo,[2)]Dept. Geophys., Science, Univ. Tokyo,[3)]NICT,[4)]REPPU code Institute

Observations of G-type stars indicate that the young Sun emitted stronger X-ray and extreme ultraviolet (XUV) radiation and stronger solar wind than the present Sun (Tu et al., 2005; Wood et al., 2002). Strong solar activity enhance particularly ion escape from a planet and ion escape is one of the candidate processes which have contributed to atmospheric escape and climate change on Mars. However, there is an uncertainty in the stellar XUV flux and the stellar during the early period. To understand and constrain the role of ion escape on ancient Mars, it is needed to investigate how ion escape depends on ancient solar XUV flux and solar wind conditions.
We investigated ion escape from Mars under ancient solar XUV flux and solar wind conditions based on multispecies magnetohydrodynamics (MHD) model of Terada et al. (2009). We assumed two solar XUV conditions: the XUV10 condition where the XUV flux is 10 times higher than the present flux, and the XUV50 condition where the XUV flux is 50 times higher than the present flux. For the solar wind, we also assumed two different conditions. One is the ordinary solar wind conditions where the solar wind density is 70 cm^{-3}, the solar wind velocity is 700 km s^{-1}, and the interplanetary magnetic field (IMF) strength is 6.58 nT, respectively. The other is the strong solar wind conditions where the solar wind density is 700 cm^{-3}, the solar wind velocity is 1400 km s^{-1}, and the IMF strength is 20 nT, respectively. The strong solar wind conditions are an analog of coronal mass ejection (CME) events. We assumed that Mars does not have an intrinsic magnetic field nor crustal magnetic fields. We conducted four simulations with different combination of the XUV conditions (XUV10 or XUV50) and the solar wind conditions (ordinary or strong).
We found that the stronger XUV flux and the stronger solar wind increase the O^+ escape rate. It was three times higher under the XUV50 condition than under the XUV10 condition and 16 times higher under the strong solar wind condition than under the ordinary solar wind condition. The strong XUV flux also increased the escape rates of O_2^+ and CO_2^+. When the XUV flux was weak, i.e. under the XUV10 conditions, however, the strong solar wind increased the O_2^+ escape rate only by a factor of two and decreased the CO_2^+ escape rate. This is because the nightside ionosphere was compressed by a strong return flow in the wake region. The strong return flow might be attributed to the plasma transport into the nightside and the magnetic reconnection in the tail region.

References

Tu, L., Johnstone, C. P., Gudel, M., & Lammer, H. (2015). The extreme ultraviolet and X-ray Sun in time: High-energy evolutionary tracks of a solar-like star. Astronomy & Astrophysics, 577(L3), 577?580. https://doi.org/10.1051/0004-6361/201526146
Wood, B. E., Muller, H., Zank, G. P., & Linsky, J. L. (2002). Measured mass-loss rates of solar-like stars as a function of age and activity. The Astrophysical Journal, 574(1), 412?425. https://doi.org/10.1086/340797
Terada, N., Kulikov, Y. N., Lammer, H., Lichtenegger, H. I. M., Tanaka, T., Shinagawa, H., & Zhang, T. (2009). Atmosphere and water loss from early Mars under extreme solar wind and extreme ultraviolet conditions. Astrobiology, 9(1), 55?70. https://doi.org/10.1089/ast.2008.0250

R009-30
Zoom meeting D ：11/2 AM2 (10:45-12:30)
11:30-11:45

Effects of the IMF direction on ion escape mechanism from Mars under weak intrinsic magnetic field conditions

#Shotaro Sakai[1),2)], Kanako Seki[3)], Naoki Terada[1)], Hiroyuki Shinagawa[4)], Ryoya Sakata[3)], Takashi Tanaka[4),5)], Yusuke Ebihara[6)]
[1)]Dept. Geophys., Science, Tohoku Univ.,[2)]PPARC, Tohoku Univ.,[3)]Dept. Earth & Planetary Sci., Science, Univ. Tokyo,[4)]NICT,[5)]ICSWSE, Kyushu Univ.,[6)]RISH, Kyoto Univ.

The planetary intrinsic magnetic field is critical when considering the atmospheric escape from planets. The strength of the intrinsic magnetic field particularly affects the interaction between solar wind and terrestrial-type planets (e.g., Seki et al., 2001), and it changes the escape mechanism. The terrestrial global magnetic field has also experienced strength changes (e.g., Guyodo & Valet, 1999) and reiterated reversals over 4.6 billion years (Ga) that could have affected the surface environment of planets. It is believed that ancient Mars had a global intrinsic magnetic field of interior origin and the magnetic field decayed by ~3.9 Ga (Acuna et al., 1999). One of the pieces of evidence that ancient Mars had an intrinsic field is the existence of a "crustal magnetic field" (Acuna et al., 1999). Present-day Mars leaves the magnetism in the crust mainly in the southern hemisphere, which is called the crustal magnetic field. Sakai et al. (2018) investigated the effect of a weak intrinsic magnetic field at the Martian equatorial surface on the escape mechanism. It was shown that the existence of the weak field results in an enhancement of the ion escape rate. A parker-spiral IMF was however used in order to obtain the escape rate in this earlier study.

This paper investigates the effects of the IMF direction on the ion escape mechanism from a Mars-like planet that has a northward weak intrinsic magnetic field on the equator. The northward, southward, and Parker-spiral IMFs under present solar wind conditions are compared based on multispecies magnetohydrodynamics simulations. In the northward IMF case, molecular ions es-cape from the high-latitude lobe reconnection region, where ionospheric ions are transported up-ward along open field lines. Oxygen ions originating either in the ionosphere or oxygen corona es-cape through a broader ring-shaped region. In the southward IMF case, the escape flux of heavy ions increases significantly and has peaks around the equatorial dawn and dusk flanks. The draped IMF can penetrate into the subsolar ionosphere by erosion, and the IMF becomes mass-loaded as it is transported through the dayside ionosphere. The mass-loaded draped IMF is carried to the tail, contributing to ion escape. The escape channels in the northward and southward IMF cases are different from those in the Parker-spiral IMF case. The escape rate is the lowest in the northward IMF case and comparable in the Parker-spiral and southward IMF cases. In the northward IMF case, a weak intrinsic dipole forms a magnetosphere configuration similar to that of Earth, quenching the escape rate, while the Parker-spiral and southward IMFs cause reconnection and erosion, promoting ion escape from the upper atmosphere.

This paper also presents the dependence of the escape mechanism on the IMF clock angle be-cause the escape mechanism for the purely northward and southward IMF conditions has currently been focused.

References:

Acuna, M., Connerney, J. E. P., Ness, N. F., Lin, R. P., Mitchell, D., Carlson, C. W., et al. (1999). Global distribution of crustal magnetization discovered by the Mars Global Surveyor MAG/ER experiment, Science, 284, 790-793. https://doi.org/10.1126/science.284.5415.790

Guyodo, Y., & Valet, J. ?P. (1999). Global changes in intensity of the Earth's magnetic field during the past 800 kyr. Nature, 399, 249-252. https://doi.org/10.1038/20420

Sakai, S., Seki, K., Terada, N., Shinagawa, H., Tanaka, T., & Ebihara, Y. (2018). Effects of a weak intrinsic magnetic field on atmospheric escape from Mars. Geophys. Res. Lett., 45, 9336-9343. https://doi.org/10.1029/2018GL079972

Seki, K., Elphic, R. C., Hirahara, M., Terasawa, T., & Mukai, T. (2001). On atmospheric loss of oxygen ions from Earth through magnetospheric processes. Science, 291, 1939-1941. https://doi.org/10.1126/science.1058913

R009-31
Zoom meeting D ：11/2 AM2 (10:45-12:30)
11:45-12:00

Study of proton escape from Mars based on MAVEN observations

#Yuki Mori[1)], Kanako Seki[1)], Shotaro Sakai[2)], Takuya Hara[3)], David A. Brain[4)], James P. McFadden[3)], Jasper S. Halekas[5)], Gina DiBraccio[6)], Francis G. Eparvier[7)], Bruce M. Jakosky[7)]
[1)]Dept. Earth & Planetary Sci., Science, Univ. Tokyo,[2)]Dept. Geophys., Science, Tohoku Univ.,[3)]SSL, UC Berkeley,[4)]LASP, Univ. of Colorado at Boulder, USA,[5)]Dept. Phys. & Astron., Univ. Iowa,[6)]NASA GSFC,[7)]LASP, CU Boulder

Mars is considered to have had water on surface in ancient days, while there is no surface water at present. Escape of atmospheric gases to space is considered to play an important role in this climate change. Particularly, hydrogen loss is closely related to the water content on Mars. Its main mechanism is thought to be Jeans escape of hydrogen atoms, which are dissociated from hydrogen molecules, sourced from odd-hydrogen reactions with near-surface water vapor. Since the molecular hydrogen is long-lived, the seasonal variation of hydrogen escape is predicted to be typically less than a factor of two (Krasnopolsky, 2002). However, Halekas (2017) reported unexpectedly large (about one order of magnitude) seasonal variations in the hydrogen corona. The cause of the large seasonal variation is not understood. A candidate mechanism is rapid transport of water to upper atmosphere due to the Martian dust storms. The enhancement of the hydrogen corona will increase the proton escape originated from the neutral hydrogen. In order to assess the hypothesis, we investigated proton escape from Mars based on MAVEN (Mars Atmosphere and Volatile EvolutioN) observations from November 2014 to March 2019. We also investigated if the seasonal variation depends on size of the dust storms by comparing MY32, 33 and 34, since Martian global dust storm occurred only in MY34. The result shows that planetary proton density in the optical wake and solar wind regions has a seasonal variability, and the variations in MY32, 33 and 34 are similar. It suggests that the size of dust storm does not affect proton escape. The results of the statistical analysis show that the variations in the wake region are more than one order, while those in the solar wind region are small. In order to understand the cause of the large seasonal variation in the wake region, we investigated proton density in the ionosphere during the same period. Based on comparison between proton observations in the ionosphere and wake region, we will discuss possible causes of seasonal variation of proton escape in the wake.
References:
Krasnopolsky (2002), J. Geophys. Res., doi:10.1029/2001JE001809. 5128.
Halekas (2017), J. Geophys. Res. Planets, doi: 10.1002/2017JE005306

R009-32
Zoom meeting D ：11/2 AM2 (10:45-12:30)
12:00-12:15

Seasonal variation of dayside ionospheric compositions coupled with neutral upper atmosphere on Mars

#Nao Yoshida[1)], Naoki Terada[2)], Hiromu Nakagawa[3)], David A. Brain[4)], Shotaro Sakai[1)]
[1)]Dept. Geophys., Grad. Sch. Sci., Tohoku Univ.,[2)]Dept. Geophys., Grad. Sch. Sci., Tohoku Univ.,[3)]Geophysics, Tohoku Univ.,[4)]LASP, Univ. of Colorado at Boulder, USA

The Martian thermosphere-ionosphere is a source for atmospheric escape, which is affected by both the lower-middle atmosphere and external forces. Escape rates of planetary ions from Mars change responding to the change in the solar wind and solar EUV radiation (e.g., Lundin et al., 2008a; Dubinin et al., 2017a; Dong et al., 2017), although a connection between the compositions of escape ions and ionospheric ions is an open question. Besides, recent studies suggest an impact of the lower-middle atmospheric variability on the upper atmosphere. Jakosky et al. (2017) and Slipski et al. (2018) showed a substantial variation of the homopause altitude on Mars. In addition, Yoshida et al. (under review) suggested that variations of dayside homopause altitude and N_2/CO_2 at 140 km altitude are mainly controlled by inflation and contraction of the lower atmosphere due to a change in solar heating with the Sun-Mars distance. N_2/CO_2 at 140 km varies in the range of 0.02 and 0.20, which is associated with the variations of homopause altitude. The change of atmospheric composition in the lower thermosphere would affect ionospheric composition because they are coupled with each other through photochemistry. In this study, we aim to investigate the coupling of atmospheric composition in the thermosphere and ionosphere by in-situ observations.
Seasonal variations of atmospheric compositions in the dayside thermosphere and ionosphere have been investigated using data from December 2014 to March 2018 obtained by Neutral Gas and Ion Mass Spectrometer (NGIMS) on Mars Atmosphere and Volatile EvolutioN (MAVEN). In the thermosphere, densities of CO_2, N_2, and O show seasonal sinusoidal variations. Higher values appear during perihelion and lower values during aphelion. CO_2 at 200 km altitude varies in the range from 3.36(10^6) to 1.74(10^8) cm^{-3}. This can be explained by inflation and contraction of the lower atmosphere (Yoshida et al., under review). In the ionosphere, the seasonal sinusoidal trend is also found in the CO_2^+ number density, associated with the variation of neutral CO_2 in the thermosphere. On the other hand, N^+ density shows the opposite sinusoidal trend to CO_2^+. This can be explained by the loss process of N^+, which reacts with CO_2 by the charge exchange. The vertical structures of ion species between 150 and 250 km altitude show a clear seasonal variation in the whole altitude range for CO_2^+ and O_2^+. However, it is noteworthy that the seasonal variation of vertical profiles of O^+ is not obvious. Under the photochemical equilibrium of the ionospheric layer below ~200 km, we have evaluated our results discussed above. We find that the significant variation of CO_2 associated with atmospheric inflation and contraction can explain the seasonal variations of ionospheric species, CO_2^+, O_2^+, and O^+. On the other hand, our result also shows a strong depletion of O_2^+ and O^+ between 150 and 250 km altitude during a dust storm event (Ls ~300 in MY 33). Our result reveals that different behavior of ionospheric species during the dust storm can be explained by a significant decrease of neutral O density in the thermosphere during the dust season.

R009-33
Zoom meeting D ：11/2 PM1 (13:45-15:30)
13:45-14:00

In situ observations of ions and magnetic field around Phobos: Mass Spectrum Analyzer (MSA) for Mars Moons eXploration (MMX)

#Shoichiro Yokota[1)], Naoki Terada[2)], Ayako Matsuoka[3)], Naofumi Murata[5)], Yoshifumi Saito[4)]
[1)]Osaka Univ.,[2)]Dept. Geophys., Grad. Sch. Sci., Tohoku Univ.,[3)]Kyoto University,[4)]ISAS,[5)]JAXA

The Mars Moons Exploration (MMX) mission will conduct remote-sensing and in-situ measurements and sample return for two primary science goals: 1) Reveal the origin of Mars' moons and gain a better understanding of planetary formation and material transport in the solar system; and 2), Observe governing processes of the Martian system to gain new insight on the history of the Mars system evolution. The science objectives are not only to reveal the origin of the Martian moons but also to understand physical processes in the Martian environment for investigating co-evolution of the Martian-moons system.
Mass Spectrum Analyzer (MSA) for the MMX mission will measure ions from the surface of the moons and Martian atmosphere with monitoring the solar wind ions and magnetic field. The MSA science investigation is designed to address MMX science goals related to in-situ ion and magnetic field observations in the Martian environment. To address the science goal 1), MSA will measure secondary ions such as Mg+, Si+, and Fe+ emitted from the Phobos surface, as well as O+, OH+, H2O+, and H3O+, which originate from ice inside the Phobos if they exist. For the science goal 2), MSA will perform observations of incident ions to Phobos (H+ and He++ of the solar wind and O+, O2+, etc. of the escaping Martian atmospheric ions), scattered solar wind ions, and emitted secondary ions.
We present the goals of the MSA science investigation, the conceptual design of the MSA instrumentation, and the current status of the development.

R009-34
Zoom meeting D ：11/2 PM1 (13:45-15:30)
14:00-14:15

Molecular Ion Contribution to the Polar Plume from Mars and its Dependence on Solar Wind Parameters

#Kotaro Sakakura[1)], Kanako Seki[1)], Shotaro Sakai[2)], Ryoya Sakata[1)], Hiroyuki Shinagawa[3)], David A. Brain[4)], James P. McFadden[5)], Jasper S. Halekas[6)], Gina DiBraccio[7)], Bruce M. Jakosky[8)], Naoki Terada[9)], Takashi Tanaka[10)]
[1)]Dept. Earth & Planetary Sci., Science, Univ. Tokyo,[2)]Dept. Geophys., Science, Tohoku Univ.,[3)]NICT,[4)]LASP, Univ. of Colorado at Boulder, USA,[5)]SSL, UC Berkeley,[6)]Dept. Phys. & Astron., Univ. Iowa,[7)]NASA GSFC,[8)]LASP, CU Boulder,[9)]Dept. Geophys., Science, Tohoku Univ.,[10)]REPPU code Institute

Mars once had water on its surface about 4 billion years ago, but there is no liquid water on the surface at present. Escape of the atmosphere to space is considered as the main cause of this climate change. However, the mechanism of the large amount of atmospheric loss is far from understood. Ion escape is one of the important candidates of the loss mechanism. There are three channels of the ion escape, namely, tailward escape, pickup ion, and polar plume. Polar plume ions are accelerated by the solar wind convection electric field and escape to positive E hemisphere of the Mars-Sun-Electric field (MSE) coordinates. It is estimated by Dong et al. (2017) that the escape rate of O^+ plume is 20-30% of the total O^+ escape depending on the solar EUV radiation. The rate is not negligible in order to understand the ion loss from Mars. Molecular ions in the polar plume should also be studied since it is shown that main escape species is O_2^+ for tailward escape by Inui et al. (2019). We recently reported a CO_2^+-rich plume event on August 28, 2015. Peak flux of CO_2^+ was 4.2×10^6 $cm^{-2}s^{-1}$, which is about one order of magnitude higher than the average flux of O^+ in the polar plume reported by Dong et al. (2017). Such high escape flux is unexpected because CO_2^+ is a minor component at high-altitude ionosphere due to its small scale height. To fully understand the mechanism of the polar plume, it is important to study the composition of the polar plumes.
In order to investigate relationship between a CO_2^+-rich plume event and solar wind (SW) conditions, we conducted a statistical study. We analyzed data obtained by STATIC (Supra Thermal and Thermal Ion Composition), MAG (magnetometer) and SWIA (Solar Wind Ion Analyzer) onboard MAVEN (Mars Atmosphere and Volatile EvolutioN) from Nov. 28, 2014 to Oct. 11, 2019. STATIC measures ion distribution functions with mass discrimination. In order to derive CO_2^+ number density, we use the fitting method invented by Inui et al. (2018). By fitting a log-normal distribution to O_2^+ count data, we remove O_2^+ contamination in the CO_2^+ mass range.
The results show that CO_2^+ plume events tend to be observed under high solar wind dynamic pressure and strong electric field conditions. This result is consistent with hypothesis that CO_2^+ plume is caused by deep penetration of the solar wind convection electric field due to the high solar wind dynamic pressure. On the other hand, observation frequency of O_2^+ plume events does not show such dependences on the solar wind parameters. This is probably because O_2^+ is abundant near the ionopause enough to create O_2^+ plumes regardless of the solar wind conditions. The results also show that correlations between the escape flux of CO_2^+ plume and solar wind parameters is weak. One possible reason of this weak correlation is the large orbit-to-orbit flux variation depending on whether MAVEN passes “hot spot" of the plume or not. In order to assess this hypothesis, we will report the results of statistical trajectory tracings in MHD fields obtained under different solar wind conditions.
References
Dong, Y., et al. (2017), J. Geophys. Res. Space Phys., 122, 4009?4022, doi:10.1002/2016JA023517
Inui, S., et al. (2018), Geophys. Res. Lett., 45, 5283?5289, doi:10.1029/2018GL077584
Inui, S., et al. (2019). J. Geophys. Res. Space Phys., 124, 5482?5497. doi:10.1029/2018JA026452

R009-35
Zoom meeting D ：11/2 PM1 (13:45-15:30)
14:15-14:30

A survey of ion jets within current sheets in the vicinity of Mars with MAVEN

#Yuki Harada[1)], Jasper S. Halekas[2)], Shaosui Xu[3)], Gina DiBraccio[4)], Suranga Ruhunusiri[5)], Takuya Hara[6)], James P. McFadden[6)], Jared R. Espley[4)], David L. Mitchell[6)], Christian Mazelle[7)]
[1)]Dept. of Geophys., Kyoto Univ.,[2)]Dept. Phys. & Astron., Univ. Iowa,[3)]SSL, UCB,[4)]NASA GSFC,[5)]Univ. of Iowa,[6)]SSL, UC Berkeley,[7)]CNRS,IRAP

We present a survey of ion jets observed during current sheet crossings by MAVEN in the near Mars space. We develop a fully automated algorithm that identifies current sheet crossings along with ion jets detected during the crossings, thereby utilizing a large volume of currently available MAVEN data accumulated from over 10,000 orbits. We focus on current sheets located in the Martian magnetosphere (defined as the region below the ion composition boundary in this study). Our statistical results show that (i) both sunward and anti-sunward ion jets embedded within current sheets are widely distributed around Mars, (ii) average magnetic field configuration and topology observed concurrently with the ion jets are consistent with those expected for reconnecting current sheets, (iii) the jet occurrence appears to be independent of upstream driver conditions, and (iv) most of the identified current sheets are thin with half-thickness comparable to ion inertial lengths and are embedded in low beta (<1) plasma. The apparent independence of ion jet occurrence from upstream drivers (iii) may be explained by the result (iv) that the two known conditions for reconnection onset (current sheet thickness and beta difference-magnetic shear relationship) could be satisfied for most of the identified current sheets irrespective of the solar wind conditions. We discuss potential implications of these results for the dynamics of the Martian magnetosphere.

R009-36
Zoom meeting D ：11/2　PM1　(13:45-15:30)
14:30-14:45

火星地殻残留磁場周辺で観測される周期的電子注入の研究

#加藤　倫生 [1),]原田　裕己 [2)]
[1)]京大・理・地球惑星,[2)]京大・理・地球惑星

Investigation of periodic electron injection observed in Martian crustal magnetic fields

#Michio Kato[1)], Yuki Harada[2)]
[1)]Dept. of Geophys., Kyoto Univ.,[2)]Dept. of Geophys., Kyoto Univ.

Mars has no global intrinsic magnetic field, but it has relatively strong crustal remanent magnetic fields. A complex magnetosphere is formed by the solar wind interaction with these localized crustal magnetic fields and with the upper atmosphere of Mars. If electrons get injected impulsively for some reason from the adjacent plasma into closed magnetic field lines formed above the strongly magnetized areas, it is expected that energy-time dispersed electron signatures will be observed as they drift in an energy-dependent manner in the direction perpendicular to the magnetic field while bouncing between the mirror points. These energy-time dispersed electron signatures were actually measured by the Mars Atmosphere and Volatile EvolutioN (MAVEN) mission. It has been reported that the energy-time dispersed electron signatures sometimes occur periodically for multiple times in succession, and the generation mechanism of the periodicity has not been clarified yet. In this study, we investigate the characteristics of the periodic electron energy-time dispersion observed in the crustal magnetic fields of Mars using the solar wind electron analyzer (SWEA) and magnetometer (MAG) onboard MAVEN. We conducted a preliminary survey of the periodic events from the MAVEN data obtained from September 2014 to August 2019 at altitudes from 200 km to 1000 km and latitudes of about 20 degrees north and south. As a result, we identified 92 cases in which electron energy-time dispersion was observed for multiple times in succession. We investigated the relationship between the electron injection interval and various parameters. Based on our analysis, there was no clear correlation of the periodicity with the geographic location and the solar zenith angle of the event occurrence, but the injection periods were correlated with the upstream solar wind parameters. This result suggests that the period of electron injection could be related to the waves generated in the upstream solar wind.

火星は全球的な固有磁場を持たず、地殻に比較的強い残留磁場を残すのみである。そのような偏在した地殻残留磁場および火星上層大気と太陽風の相互作用によって複雑な磁気圏を形成している。強い地殻磁場周辺に形成される閉じた磁力線になんらかの要因で外部から電子が瞬間的に注入された場合、ミラー点の間をバウンスしながら磁場と垂直方向にエネルギー依存を伴うドリフト運動をするために電子のエネルギー分散が見られることが予想され、これまでの観測により実測されている。
そのようなイベントの中にエネルギー分散が複数回連続して発生しているものが報告されているが、その発生機構は未だ解明されていない。本研究では、火星探査機 MAVEN(Mars Atmosphere and Volatile EvolutioN)に搭載された太陽風電子分析器(SWEA)と磁力計 (MAG)を用いて火星地殻磁場付近で観測される周期的電子エネルギー分散の特徴を明らかにする。
2014 年 9 月から 2019 年 8 月の期間で、高度 200km から 1000km、北緯約 20 度以南の範囲で解析を行ったところ、電子エネルギー分散が複数回連続して観測された例が 92 例確認された。これらのイベントについて電子注入の時間間隔と各種パラメータとの関係を調べた結果、電子注入周期はイベント発生位置・太陽天頂角とは相関がなく、上流太陽風パラメータに相関が認められた。この結果は、電子注入の周期が上流太陽風で発生する波動に起因することを示唆する。

R009-37
Zoom meeting D ：11/2 PM1 (13:45-15:30)
14:45-15:00

Statistical properties of solar energetic electron penetration into the Martian upper atmosphere observed by MAVEN

#Kanako Seki[1)], Takuya Hara[2)], David A. Brain[2),3)], Robert J. Lillis[2)], Davin E. Larson[2)], David L. Mitchell[2)], Gina DiBraccio[4)], Janet G. Luhmann[2)], Bruce M. Jakosky[5)]
[1)]Dept. Earth & Planetary Sci., Science, Univ. Tokyo,[2)]SSL, UC Berkeley,[3)]LASP, Univ. of Colorado at Boulder, USA,[4)]NASA GSFC,[5)]LASP, CU Boulder

The diffuse aurora observation at Mars in the region where the crustal magnetic field is absent, indicates penetration of the high-energy electrons of ~100 keV down to the altitudes around 70 km along the draped IMF around the planet [Schneider et al., 2015; 2018]. However, how the draped magnetic field configuration around Mars controls the SEP (solar energetic particle) electron penetration to the atmosphere is far from understood. Moreover, global simulations of the solar-wind-Mars interaction have shown that the existence of the crustal magnetic fields primarily in the southern hemisphere results in the complexed magnetic structure around entire Mars [e.g., Luhmann et al., 2015].
In this study, we investigated SEP events observed by MAVEN from December 2014 to October 2017 in order to investigate effects of the magnetic field structure in the ionosphere, including both the crustal magnetic fields and penetrating draped IMF, on SEP pitch angle distributions and energy dependent loss into the atmosphere. The pitch angle (PA) distributions of the high-energy (30-210 keV) electrons observed in the Martian ionosphere are analyzed in details. In order to achieve a good coverage in the 2-D (PA-energy) phase space, data obtained during a SEP event is accumulated and binned. Using the elevation angle of the local magnetic field, we also sorted the data so as to investigate the SEP electron loss below the MAVEN periapsis (~150 km altitude). The obtained PA distributions in the ionosphere are compared with the distributions of the source electrons in the magnetosheath. For some of the strong SEP events, one-to-one correspondence of the SEP distributions to the strength and dip angle of the local magnetic field was investigated.
The results show that the field-aligned component is pronounced for the penetrating electrons and it does not significantly depend on the initial PA distributions in the magnetosheath. The highest energy of the SEP electrons lost into the Martian atmosphere depends on the magnetic field configuration draped around the planet. The SEP electron penetration depleted in the region of the strong crustal magnetic field. Its loss into the atmosphere tend to be pronounced in the nightside, suggesting the deeper penetration of draped magnetic fields in the nightside than dayside. We will also report on the energy dependent penetration seen in some SEP events and discuss role of the magnetic field to determine the precipitation flux of SEP electrons into the Martian atmosphere.
References:
Schneider et al., Science, 350, 6261, doi:10.1126/science.aad0313, 2015.
Schneider et al., Geophys. Res. Lett., 45, 7391?7398. doi:10.1029/2018GL077772, 2018.
Luhman et al., Geophys. Re. Lett, 42, doi:10.1002/2015GL066122, 2015.